Redox Regulation of Brain Selective Kinases BRSK1/2: Implications for Dynamic Control of the Eukaryotic AMPK family through Cys-based mechanisms

George N. Bendzunas [1#,] Dominic P Byrne [2#,] Safal Shrestha [3], Leonard A Daly [2,4], Sally O. Oswald [2,4], Samiksha Katiyar [1], Aarya Venkat [1], Wayland Yeung [1,3], Claire E Eyers [2,4], Patrick A Eyers* [3], Natarajan Kannan* [1,2]

# Equal contributions

[1] Department of Biochemistry and Molecular Biology, University of Georgia, Athens, GA 30602, USA [2] Department of Biochemistry, Cell and Systems Biology, Institute of Systems, Molecular and Integrative Biology, University of Liverpool, Liverpool L69 7ZB, UK. [3] Institute of Bioinformatics, University of Georgia, Athens, GA 30602, USA. [4] Centre for Proteome Research, Institute of Systems, Molecular and Integrative Biology, University of Liverpool, Liverpool L69 7ZB, UK

*Correspondence to: Natarajan Kannan, Email: nkannan@uga.edu or Patrick Eyers, Email: patrick.eyers@liverpool.ac.uk

Abstract

In eukaryotes, protein kinase signaling is regulated by a diverse array of post-translational modifications (PTMs), including phosphorylation of Ser/Thr residues and oxidation of cysteine (Cys) residues. While regulation by activation segment phosphorylation of Ser/Thr residues is well understood, relatively little is known about how oxidation of cysteine residues modulate catalysis. In this study, we investigate redox regulation of the AMPK-related Brain-selective kinases (BRSK) 1 and 2, and detail how broad catalytic activity is directly regulated through reversible oxidation and reduction of evolutionarily conserved Cys residues within the catalytic domain. We show that redox-dependent control of BRSKs is a dynamic and multilayered process involving oxidative modifications of several Cys residues, including the formation of intra-molecular disulfide bonds involving a pair of Cys residues near the catalytic HRD motif and a highly conserved T-Loop Cys with a BRSK-specific Cys within an unusual CPE motif at the end of the activation segment. Consistently, mutation of the CPE-Cys increases catalytic activity *in vitro* and drives phosphorylation of the BRSK substrate Tau in cells. Molecular modeling and molecular dynamics simulations indicate that oxidation of the CPE-Cys destabilizes a conserved salt bridge network critical for allosteric activation. The occurrence of spatially proximal Cys amino acids in diverse Ser/Thr protein kinase families suggests that disulfide mediated control of catalytic activity may be a prevalent mechanism for regulation within the broader AMPK family.

Introduction

Protein kinases are crucial components in cellular signaling networks, functioning as reversible molecular switches that orchestrate various biological processes. There are over 500 protein kinases encoded in the human genome that coordinate a wide range of cellular processes by catalyzing the transfer of a phosphate group from ATP to a hydroxyl group on the amino acid side chains of serine, threonine, or tyrosine residues in protein substrates (Manning et al. 2002). By catalyzing the reversible post-translational phosphorylation of Ser/Thr and Tyr residues of substrate proteins, protein kinases serve as signaling integrators that govern most aspects of eukaryotic life. Consequently, there exists a biological imperative to tightly control the catalytic activities of protein kinases, through cyclical phosphorylation of conserved amino acids, protein-protein interactions, and other regulatory post-translational modifications (PTMs). One essential mechanism governing kinase activity is the reversible phosphorylation of conserved amino acid residues within the activation loop, henceforth referred to as the T-Loop (Nolen, Taylor, and Ghosh 2004). In the inactive, unphosphorylated state, the T-Loop adopts a wide range of conformations, including conformations that obstruct substrate binding (Engh and Bossemeyer 2001). Phosphorylation of the activation loop induces an active spatial conformation that is typically more amenable to both binding and enzymatic phosphorylation of protein substrates, and this modification is prevalent across the kinase superfamily (Faezov and Roland L. Dunbrack 2023). Conversely, the removal of phosphate groups in this region by phosphatases (dephosphorylation) usually reverts kinases to an inactive state, generating a reversible switch to turn “on” and “off” kinase-dependent signaling pathways. More recently we hypothesized that ~10% of the Ser/Thr human kinome may also be subject to a conserved form of redox-dependent regulation, including key members of the CAMK, AGC, and AGC-like families of kinases through reversible oxidation of an evolutionarily conserved Cys residue, which lies adjacent to the critical regulatory phosphorylation site on the activation loop (T-loop +2 position) (Byrne et al. 2020).

Understanding the molecular mechanisms underlying kinase regulation by redox-active Cys residues is fundamental as it appears to be widespread in signaling proteins (Xiao et al. 2020; Corcoran and Cotter 2013; Cao et al. 2023) and provides new opportunities

67 to develop specific covalent compounds for the targeted modulation of protein kinases
68 (Weisner et al. 2015). Moreover, redox-active Cys are major sensors of **R**eactive
69 **O**xygen **S**pecies (ROS), such as superoxide and peroxide, which function as
70 endogenous secondary messengers to regulate various cellular processes (Schieber
71 and Chandel 2014; Wani et al. 2011). In particular, the high cell permeability of H_2O_2
72 relative to other ROS species allows it to be sensed intracellularly by reactive Cys,
73 which can differentially impact protein function and cellular localization (Lennicke et al.
74 2015; Rhee et al. 2005). Chemically accessible and reactive Cys residues can transition
75 through several redox states, such as the transient sulfenic acid species (Cys-SOH) and
76 higher order, 'irreversible', sulfinic and sulfonic forms (Cys-SO_2H and Cys-SO_3H)
77 (Forman et al. 2017; Gupta and Carroll 2014). Importantly, in the context of allosteric
78 protein redox regulation, the sulfenic oxidized Cys species can form disulfide linkages
79 with other reactive Cys residues, whilst a sulfenic derivative has also been observed to
80 be stabilized through the formation of a cyclic sulfenamide for tyrosine phosphatase
81 PTP1B (van Montfort et al. 2003; Salmeen et al. 2003). The chemical reactivity, and
82 thus biological susceptibility, of an individual Cys residue to oxidative modification is
83 contingent on the intrinsic pK_a value (where K_a is the acid dissociation constant), which
84 in turn is influenced by networks of interacting amino acids (including phosphorylated
85 amino acids), solvent accessibility, protein-protein interactions, and protein structural
86 dynamics (Poole 2015; Xiao et al. 2020; Soylu and Marino 2016). Unlike
87 phosphorylation, which allosterically communicates with distal sites through positively
88 charged residues that coordinate the phosphate group, it is largely unclear how the
89 redox state of a T-loop localized Cys residue may alter the catalytic activity of a kinase
90 (Garrido Ruiz et al. 2022), although a change in the activation segment conformation is
91 a likely outcome, as demonstrated by careful analysis of Ser/Thr kinases, notably
92 members of the AGC-family kinase AKT (Su et al. 2019).
93 The human AMPK-related kinase (ARK) family, consisting of 14 members (termed
94 BRSK1-2, NUAK1-2, SIK1-3, MARK1-4, MELK, and AMPKα1 and AMPKα2) are
95 fundamental regulators of cellular metabolism, growth, differentiation, and polarity (Shao
96 et al. 2014; Byrne et al. 2020; Shirwany and Zou 2014; Zmijewski et al. 2010), and
97 BRSK1/2 function upstream of redox-based signaling to the pleiotropic transcription

factor Nrf2 (Tamir, Drewry, et al. 2020; Tamir, Bowman, et al. 2020). Like other ARK members, BRSK1/2 possess similar structural organization, consisting of an N-terminal serine/threonine catalytic (kinase) domain, which is followed by a ubiquitin-associated (UBA) domain, a C-terminal spacer, and in some members, a kinase-associated (KA1) domain (Bright, Thornton, and Carling 2009) (Fig 1a). In addition to sharing structural homology, all ARKs (except for MELK) are known to be activated by phosphorylation on their T-Loop by the common upstream regulator LKB1, which is constitutively catalytically active in cells (Lizcano et al. 2004). All of the ARKs contain an activation loop 'T-loop + 2 Cys' residue, which can be prognostic for redox regulation (Byrne et al. 2020), and the catalytic activities of several members have been demonstrated experimentally to be modulated by ROS, including the nominative member, AMPKα, which is both directly and indirectly regulated by redox-state (Auciello et al. 2014; Hinchy et al. 2018; Choi et al. 2001; Shirwany and Zou 2014; Shao et al. 2014). However, the precise mechanisms whereby various ARKs are regulated under redox conditions remain obscure and are likely to be context specific.

The Brain Specific Kinases (BRSKs, also termed Synapses of Amphids Defective [SAD] kinases), consist of two paralogs in vertebrates, termed BRSK1 and BRSK2, and are among the least well-studied of the ARK family (Nie et al. 2012). However, like all other members of the ARK family, BRSKs are downstream signaling targets of the Ser/Thr kinase LKB1 and also have the potential to be regulated 'upstream' by CAMKII, PAK1, and PKA, suggesting signal-dependent phosphorylation as a central regulatory mechanism (Alessi, Sakamoto, and Bayascas 2006; Lizcano et al. 2004; Nie et al. 2012; Bright, Carling, and Thornton 2008). BRSKs are highly expressed in the brain and central nervous system of model organisms, where they exhibit both distinct and redundant molecular functions (Kishi et al. 2005; Nakanishi et al. 2019); furthermore, they are implicated in several human pathologies, in particular neurodevelopmental disorders such as autism spectrum disorder (Saiyin et al. 2017; Li et al. 2020; Deng et al. 2022).

In the current study, we identify a new dominant mechanism for regulation of BRSKs through oxidative modification of conserved Cys residues within the kinase domain. We

demonstrate that the catalytic activities of both BRSK1 and BRSK2 are fine-tuned through oxidative modification of the T-Loop +2 Cys residue, which communicates with a BRSK-specific Cys residue in the APE motif (CPE in BRSKs) within the activation segment. We provide evidence that the T-Loop Cys forms disulfide bonds with the 'CPE' motif Cys and that mutating the CPE-Cys to an alanine increases BRSK activity relative to the wild-type (WT) enzyme. Using a combination of biochemical analysis, structural modeling, and molecular dynamics simulations, we identify regulatory roles for these BRSK-conserved Cys residues and characterize novel intramolecular disulfide-links, providing new insights into BRSK1/2 regulation and the broader AMPK family regulation. Together, these findings highlight complex regulatory processes for BRSK1/2 that are dependent on both phosphorylation and Cys-redox modulation, with broad implications for the other dozen members of the ARK family.

Methods

Recombinant proteins and general reagents

All purchased biochemicals were of the highest purity available, and all recombinant proteins were analyzed by intact mass-spectrometry to confirm the species present. Active, recombinant full-length BRSK1 (2-778) and BRSK2 (2-674) proteins purified from insect Sf21 cells were purchased from MRC PPUU reagents (University of Dundee). Active recombinant LKB1/STRADα/MO25α was purchased from Merck. Gateway pENTR plasmids encoding full length human BRSK1 & BRSK2 were generated as part of the NIH common fund initiative to Illuminate the Druggable Genome (IDG) and was a gift from Dr. Ben Major (Washington University, St. Louis). Antibodies for BRSK1, BRSK2, DYKDDDDK (D6WB5) Tag, Phospho-AMPKα (Thr172), HA-Tag (C29F4), 6XHiS tag and GAPDH were from Cell Signaling Technology. Antibodies for Phospho-Tau and GFP were from Invitrogen. The glutathione antibody was obtained from Abcam.

Cloning, Gateway Recombination and Site Directed Mutagenesis

BRSK1 and 2 were cloned into pDest vectors (to express N-terminal Flag or HA tagged proteins) using the Gateway LR Clonase II system (Invitrogen) as per the manufacturer's instructions. pENtR clones were obtained in the form of a Gateway-compatible donor vectors from the laboratory of Ben Major (Washington University in St. Louis). The Gateway LR Clonase II enzyme mixture mediates recombination between the attL sites on the Entry clone and the attR sites on the destination vector. BRSKs were also cloned into a pcDNA3 vector using a standard T4-ligase (NEB) protocol and expressed in frame with a 3C-protease cleavable N-terminal tandem STREP-tag. The catalytic domains of BRSK1$^{29-358}$ or BRSK2$^{14-341}$ were sub-cloned into pET28a (Novagen) to generate N-terminal hexa-His tagged plasmid constructs for expression of BRSK1/2 catalytic domains in *E. coli*. Site-directed mutagenesis was performed using standard PCR-based mutagenic procedures with the Q5 Site-Directed Mutagenesis Kit (New England Biolabs) following the manufacturer's instructions. All plasmids were validated by complete sequencing of the protein coding region.

173

174 **Recombinant BRSK expression and purification**

175 Recombinant human BRSK1$^{29-358}$ or BRSK2$^{14-341}$ proteins, or each of the indicated
176 amino acid substitutions, were produced in BL21 (DE3) pLysS *E. coli* cells (Novagen)
177 and purified in the absence of reducing agents, unless stated otherwise. BRSK1/2
178 expression was induced with 0.5 mM isopropyl-β-D-thiogalactopyranoside (IPTG) for 18
179 h at 18°C and N-terminal His6-tag fusion proteins purified by step-wise affinity
180 chromatography and size exclusion chromatography using a HiLoad 16/600 Superdex
181 200 column (GE Healthcare) equilibrated in 50 mM tris-HCl (pH 7.4), 100 mM NaCl, and
182 10% (v/v) glycerol. Where appropriate for redox assays, recombinant proteins were
183 purified under reducing conditions in the presence of 1 mM DTT, as previously
184 described (Byrne et al. 2020). BRSK proteins expressed from bacteria are
185 unphosphorylated and catalytically inactive, and were activated by incubation with 10 ng
186 of purified LKB1/STRADα/MO25α holoenzyme complex in the presence of 1 mM ATP
187 and 10 mM $MgCl_2$ for 18 h at 4°C. Phosphorylation of BRSK proteins was verified by
188 mass spectrometry and/or Western blotting analysis using a pThr^{172} AMPKα antibody,
189 which demonstrates cross-reactivity for BRSK1/2 T-Loop phosphorylation (Tamir et al.
190 2020).

191

192 **Detection of glutathionylated proteins by immunoblotting**

193 Recombinant BRSK1 and 2 (0.5 µg) were incubated with 50 mM Tris-HCl (pH 7.4) and
194 100 mM NaCl, with 10 mM GSSG or GSH for 30 min at 20°C, and glutathione-protein
195 complexes were detected by immunoblotting after nonreducing SDS-PAGE.

196

197 **BRSK1/2 Kinase assays**

198 BRSK activity assays were performed using microfluidic real-time mobility shift-based
199 assays, as described previously (Byrne et al. 2020; Byrne et al. 2016; Mohanty et al.
200 2016), in the presence of 2 µM of the fluorescent-tagged BRSK1/2 peptide substrate
201 (AMARA; 5-FAM- AMARAASAAALARRR -COOH) and 1 mM ATP. Optimal pressure and
202 voltage settings were established to improve separation of phosphorylated and
203 nonphosphorylated peptides. All assays were performed in 50 mM HEPES (pH 7.4),

204 0.015% (v/v) Brij-35, and 5 mM $MgCl_2$, and the real-time or end point degree of peptide
205 phosphorylation was calculated by differentiating the ratio of the
206 phosphopeptide:peptide. BRSK1/2 activity in the presence of different redox reagents
207 was quantified by monitoring the generation of phosphopeptide during the assay,
208 relative to controls. Data were normalized with respect to control assays, with
209 phosphate incorporation into the peptide generally limited to <20% to prevent depletion
210 of ATP and to ensure assay linearity. Recovery of BRSK activity from oxidative inhibition
211 was assessed by incubating BRSKs with 1 mM hydrogen peroxide, followed by infusion
212 of 2 mM DTT and substrate phosphorylation monitoring in real time. To account for
213 potential variability in LKB1-dependent phosphorylation of BRSK proteins, rates of
214 kinase activity (calculated as pmol phosphate incorporation per min) for each protein
215 was normalized by densitometry to the activation site of phosphorylation signal
216 (established with $pThr^{172}$ AMPKα antibodies and ImageJ software).
217

218 **Differential Scanning Fluorimetry**

219 Thermal shift assays were performed with a StepOnePlus real-time polymerase chain
220 reaction (PCR) machine (Life Technologies) using SYPRO Orange dye (Invitrogen) and
221 thermal ramping (0.3°C in step intervals between 25° and 94°C). All proteins were
222 diluted to a final concentration of 5 μM in 50 mM tris-HCl (pH 7.4) and 100 mM NaCl in
223 the presence or absence of 10 mM DTT and were assayed as described previously
224 (Foulkes et al. 2018). Normalized data were processed using the Boltzmann equation to
225 generate sigmoidal denaturation curves, and average $T_m/\Delta T_m$ values were calculated as
226 previously described (Murphy et al. 2014) using GraphPad Prism software.
227

228 **Human cell culture and treatment**

229 HEK-293T cells were cultured in Dulbecco's modified Eagle medium (Lonza)
230 supplemented with 10% fetal bovine serum (HyClone), penicillin (50 U/ml), and
231 streptomycin (0.25 μg/ml) (Lonza) and maintained at 37°C in 5% CO_2 humidified
232 atmosphere. To examine the effects of oxidative stress on BRSK activity, cells were
233 transiently co-transfected for 24 h with plasmids for expression of full-length, N-terminal
234 tagged (Flag, HA or tandem Strep tag) BRSK1/2 (or Cys-Ala mutants) and EGFP-TAU

235 (Addgene), using 3:1 polyethylenimine (average M_w, ~25,000 Da; Sigma-Aldrich) to total
236 DNA ratio (4 µg BRSK and 2 µg TAU DNA) in a single well of a 24-well culture plate. To
237 investigate inactivation of BRSK by peroxide, cells were incubated for 20 min with 10
238 mM H_2O_2, or buffer control. To establish reversibility of oxidative inhibition, cells were
239 incubated for 20 min with 10 mM H_2O_2, or buffer control followed by a 15 min incubation
240 with 20 mM reduced glutathione (GSH). In all assays, cells were subsequently washed
241 3x in PBS, harvested in bromophenol blue–free SDS sample buffer supplemented with
242 1% Triton X-100, protease inhibitor cocktail tablet, and a phosphatase inhibitor tablet
243 (Roche), or in lysis buffer (50 mM Tris-HCl (pH 7.4), 150 mM NaCl, 1 mM EDTA with 10
244 % (v/v) glycerol and 1 % (v/v) Triton X-100, with 1X protease inhibitor cocktail and 1X
245 HALT phosphatase inhibitor). Lysates were sonicated briefly and clarified by
246 centrifugation at 20 817×*g* for 20 min at 4°C, and supernatants were sampled and
247 diluted 30-fold for calculation of the protein concentration using the Coomassie Plus
248 Staining Reagent (Bradford) Assay Kit (Thermo Fisher Scientific). Cell lysates were
249 normalized for total protein concentration and processed for immunoblotting or immuno-
250 precipitation (IP).
251
252 **Liquid chromatography mass spectrometry (LC-MS) analysis BRSKs**
253 48 h post-transfection, HEK-293T cells overexpressing BRSK1 and 2 (containing an N-
254 terminal 3C cleavable tandem STREP-tag) were treated with 1 mM of the cell
255 permeable chemical oxidant pervanadate for 30 min. Cells were resuspended in ice
256 cold lysis buffer (50 mM Tris-HCl (pH 6.5), 150 mM NaCl, 10 % (v/v) glycerol, 1 % (v/v)
257 NP-40, 100 mM iodoacetamide) and disrupted by passing the cell suspension through a
258 25-gauge needle 10 times. Lysates were clarified by centrifugation at 20 817×g for 20
259 min at 4°C, and recombinant proteins were affinity precipitated using Strep-TACTIN
260 beads and physically eluted using 3C protease for subsequent MS analysis. Affinity
261 precipitated BRSK1/2 and bacterially derived recombinant proteins (10 µg) were diluted
262 (~4-fold and ~18-fold respectively) in 100 mM ammonium bicarbonate (pH 8.0)
263 containing 10 mM iodoacetamide and incubated in the dark for 30 min at room
264 temperature. Samples were subjected to an SP3-based trypsin digestion protocol
265 (adapted from, (Daly et al. 2023)), using 100 mM ammonium bicarbonate (pH 8.0) and

266 0.5 µg of Trypsin gold (Promega). Digested fractions were split 50/50, and one half was
267 treated with dithiothreitol and iodoacetamide as previously described by (Ferries et al.
268 2017). Samples were then subjected to in-house packed strong-cation exchange stage
269 tip clean up, as described by (Daly et al. 2021). Dried peptides were solubilized in 20 µl
270 of 3% (v/v) acetonitrile and 0.1% (v/v) TFA in water, sonicated for 10 min, and
271 centrifuged at 13,000x *g* for 15 min at 4 °C prior to reversed-phase HPLC separation
272 using an Ultimate3000 nano system (Dionex) over a 60-min gradient, as described by
273 (Ferries et al., 2017). For affinity precipitated BRSK preparations from human cells, all
274 data acquisition was performed using a Thermo QExactive mass spectrometer (Thermo
275 Scientific), with higher-energy C-trap dissociation (HCD) fragmentation set at 30%
276 normalized collision energy for 2+ to 4+ charge states. MS1 spectra were acquired in
277 the Orbitrap (70K resolution at 200 *m/z*) over a range of 300 to 2000 *m/z*, AGC target =
278 1e6, maximum injection time = 250 ms, with an intensity threshold for fragmentation of
279 1e3. MS2 spectra were acquired in the Orbitrap (17,500 resolution at 200 *m/z*),
280 maximum injection time = 50 ms, AGC target = 1e5 with a 20 s dynamic exclusion
281 window applied with a 10 ppm tolerance. For bacterially derived recombinant proteins,
282 all data acquisition was performed using a Thermo Fusion Tribrid mass spectrometer
283 (Thermo Scientific), with higher-energy C-trap dissociation (HCD) fragmentation set at
284 32% normalized collision energy for 2+ to 5+ charge states. MS1 spectra were acquired
285 in the Orbitrap (120K resolution at 200 *m/z*) over a range of 400 to 2000 *m/z*, AGC
286 target = 100%, maximum injection time = auto, with an intensity threshold for
287 fragmentation of 2.5e4. MS2 spectra were acquired in the Orbitrap (30k resolution at
288 200 *m/z*), maximum injection time = dynamic, AGC target = auto with a 20 s dynamic
289 exclusion window applied with a 10 ppm tolerance. For disulfide analysis (regardless of
290 sample type), raw data files were converted into mgf format using MSConvert, with peak
291 picking filter set to “2- ” and searched with the MASCOT search engine (Perkins et al.
292 1999); searching the UniProt Human Reviewed database (updated weekly, accessed
293 January 2023) (UniProt 2023) with variable modifications = carbamidomethylation (C),
294 oxidation (M), phosphorylation (ST), instrument type = electrospray ionization–Fourier-
295 transform ion cyclotron resonance (ESI-FTICR) with internal fragments from 200-2000
296 *m/z*, MS1 mass tolerance = 10 ppm, MS2 mass tolerance = 0.01 Da. The crosslinking

297 option was selected for the accessions Q8TDC3 or Q8IWQ3 with strategy set to Brute-
298 force, for InterLink, IntraLink and LoopLink for the linker “Xlink: Disulfide (C)”. For the
299 best MASCOT scoring peptide spectrum match (PSM) for a disulfide-containing peptide,
300 the mgf file was extracted from the raw file and imported into a custom R script for re-
301 drawing and manual annotation. Immunoprecipitated samples were additionally
302 analyzed using PEAKS Studio (version XPro) using the same database, mass
303 tolerances and modifications as previously described. PEAKS specific search settings:
304 instrument = Orbi-Orbi, Fragmentation = HCD, acquisition = DDA, De Novo details =
305 standard and a maximum of 5 variable PTMs possible. PEAKS PTM mode was enabled
306 and filtering parameters of De Novo score >15, -log10P(value) >30.0, Ascore >30.0.
307

308 **Phylogenetic Analysis**

309 We identified and aligned diverse BRSK-related sequences from the UniProt reference
310 proteomes database (downloaded on June 7, 2022) (UniProt 2023) using MAPGAPS
311 (Neuwald 2009). From these hits, we manually curated a diverse set of sequences, then
312 inferred a maximum-likelihood phylogenetic tree with IQ-TREE version 2.0.7 (Minh et al.
313 2020). Branch support values were generated using ultrafast bootstrap (Hoang et al.
314 2018) with 1000 resamples. The optimal substitution model was LG+R6 based on the
315 Bayesian Information Criterion as determined by ModelFinder (Kalyaanamoorthy et al.
316 2017). The consensus tree was used as our final topology. Subsequent analyses were
317 performed using the ETE3 Toolkit (Huerta-Cepas, Serra, and Bork 2016).
318

319 **Molecular Dynamics Simulations**

320 The starting model for molecular dynamics (MD) simulations was selected to provide an
321 accurate representation of the protein kinase in its active-like conformation. To achieve
322 this, we utilized an AlphaFold model of the BRSK2 kinase domain, corresponding to
323 residues 14-267, in an active-like conformation. The average pLDDT score for the
324 portion of the AlphaFold model employed in MD simulations was calculated to be
325 89.18%, indicating high confidence and accuracy (Jumper et al. 2021). Starting
326 structures were prepared using the CHARMM-GUI interface which allowed for
327 incorporation and parameterization of T-Loop phosphorylation, cysteine to alanine

328 mutation, and oxidative cysteine modification (Brooks et al. 2009; Lee et al. 2016; Jo et
329 al. 2014). Cysteine 176 (T+2) and 183 (CPE motif) were each mutated to alanine,
330 sulfenic acid, or sulfonic acid forms. The protein was solvated in a cubic box of TIP3P
331 water molecules, and counterions were added to maintain neutrality. The final systems
332 contained ~ 54,000 atoms.
333 Prior to production runs, the system was subjected to minimization and equilibration
334 protocols, using previously described parameters (Yeung et al. 2021; Venkat et al.
335 2023). Initially, a steepest descent energy minimization was performed to relax the
336 system, followed by equilibration at constant volume and temperature (NVT) and
337 constant pressure and temperature (NPT). Each equilibration stage was carried out for
338 125 ps with 1 fs time steps. Following equilibration, long-range electrostatics were
339 calculated via particle mesh Ewald (PME) algorithms using the GROMACS MD engine
340 (Van Der Spoel et al. 2005). Three 100 ns production molecular dynamics (MD)
341 replicates were conducted at a 2fs time-step using the CHARMM36 forcefield for each
342 starting model (Brooks et al. 2009). The resultant MDs were visualized with PyMOL
343 (Schrodinger 2015) and analyzed in the python environment (Michaud-Agrawal et al.
344 2011).
345
346 **SDS-PAGE and Western blotting**
347 Processed cell lysates and purified recombinant proteins were loaded onto 10% (v/v)
348 SDS-PAGE gels, separated by electrophoresis and transferred onto nitrocellulose
349 membranes using a semi-dry transfer system at 300 mA for 45 minutes. Nitrocellulose
350 membranes were blocked with 4% (w/v) Bovine Serum Albumin (BSA, Rockland) in
351 Tris-buffered saline with 0.1% (v/v) Tween-20 (TBST) for 1 h at room temperature and
352 incubated overnight at 4°C with the indicated primary antibodies. Protein was detected
353 using specific secondary IRdye conjugated antibodies (Donkey anti Rabbit IRdye800cw
354 or Goat anti Mouse IRdye680) and imaged using LI-COR Odyssey imaging system, or
355 HRP-conjugated secondary antibodies and enhanced chemiluminescence reagent
356 (Pierce ECL Plus, Thermo Fisher Scientific). All antibodies were prepared in a solution
357 of BSA dissolved in TBST and diluted according to manufacturer's instructions.

358 Reducing and non-reducing SDS-page for BRSK proteins was performed as previously
359 described (Byrne et al, 2020).

360 Two-color Western blot detection method employing infrared fluorescence was used to
361 measure the ratio of Tau phospho serine 262 to total Tau. Total EGFP Tau was detected
362 using a mouse anti GFP antibody and visualized at 680 nm using goat anti mouse
363 IRdye 680 while phospho-tau was detected using a Tau phospho serine 262 specific
364 antibody and visualized at 800 nm using goat anti rabbit IRdye 800. Imaging was
365 performed using a LI-COR Odyssey Clx with scan control settings set to 169 µm,
366 medium quality, and 0.0 mm distance. Quantification was performed using Li-COR
367 image studio on the raw image files. Total Tau to phospho Tau ratio was determined by
368 measuring the ratio of the fluorescence intensities at 800 nm (pTau) to those at 680 nm
369 (total tau) for each band. Statistical analysis was conducted in GraphPad Prism, to
370 determine significant differences between experimental groups. Data is presented as
371 mean ± standard error of the mean (SEM).

372

373 **Size Exclusion Chromatography with multi-angle Light scattering (SEC-MALS)**

374 The oligomeric state of recombinant BRSKs was characterized by in-line Size Exclusion
375 Chromatography-Multi-Angle Laser Light Scattering (SEC-MALS). Purified BRSK
376 proteins (1 mg mL^{-1}) were applied directly to a HiLoad 16/60 Superdex 200 attached to
377 an ÄKTA pure fast protein liquid chromatography (FPLC) system equilibrated in 10 mM
378 Tris-HCl pH 7.4, 150 mM NaCl at a flow rate of 0.7 mL min^{-1}. Eluted protein was
379 detected by a MALLS detector and a differential refractive index (DRI) detector (DAWN
380 HELEOS-II and Optilab TrEX; Wyatt Technology, Santa Barbara, CA, USA). Data was
381 analyzed using ASTRA v6.1 software (WYATT). The system was calibrated using BSA
382 prior to data collection with BRSK1/2 proteins.

383

384 **Results**

385 **Full-length BRSKs exhibit Redox-Sensitivity**

386 Full length BRSK kinases share similar domain architecture to other ARK family
387 members, including a ubiquitin associate domain (UBA) and kinase associated domain
388 (KA1) following their kinase domain (Fig 1a). Due to the absence of known endogenous
389 substrates selectively phosphorylated by BRSK1 or 2 (Tamir et al. 2020), we utilized a
390 EGFP-Tau overexpression system in HEK-293T cells to assess BRSK activity (Yoshida
391 and Goedert 2012). BRSK1 and 2, when co-expressed with EGFP-Tau, induced
392 substantial phosphorylation of Tau at Ser 262, a modification lost in kinase-dead (KD)
393 mutants with the catalytic aspartate in the 'HRD' motif mutated to alanine ($D146^{BRSK1}$ or
394 $D141^{BRSK2}$), as shown in Figure 1b. The catalytic output of purified full length human
395 BRSK1 & 2 purified from Sf21 cells was next monitored in real-time using a microfluidic
396 kinase assays system and a generic ARK family substrate peptide AMARA (5-FAM-
397 AMARAASAAALARRR -COOH), which is phosphorylated by BRSK1/2, but not the
398 upstream kinase LKB1. In the absence of reducing agents (buffer alone), detectable
399 peptide phosphorylation was extremely low for both kinases and ablated in the
400 presence of H_2O_2 (Fig 1c). In contrast, inclusion of DTT enhanced BRSK1 & 2 activity by
401 several orders of magnitude (Fig 1c). Moreover, H_2O_2-dependent inhibition of catalysis
402 could be reversed, and even increased relative to basal activity, with the subsequent
403 addition of a bolus of the reducing agent DTT (Fig 1c). BRSK proteins were rapidly
404 activated by DTT in a concentration-dependent manner, suggesting an obligate
405 requirement of an appropriate reducing environment in order to enable catalytic activity
406 (Fig 1d and Supp Fig 2a-b). Similarly, basal BRSK activity was inhibited by a gradient of
407 H_2O_2 (Fig 1e, Supp Fig 2c-d). Western blotting revealed a dose-dependent and
408 statistically significant decrease in BRSK-mediated pTau signal following incubation of
409 HEK-293T cells with 10 mM peroxide for 10 minutes, with little alteration in total
410 transfected Tau protein (Fig 1f). At the highest concentrations of peroxide treatment, we
411 detected a reduction in total BRSK protein levels, suggesting a potential loss of stability
412 for both kinases. Chronic oxidative stress was next stimulated by supplementing culture
413 medium with (2 U/mL) glucose oxidase to facilitate constitutive steady-state generation

414 of H_2O_2 (Askoxylakis et al. 2011, Mueller et al. 2009, Truong et all, 2016). This revealed
415 a time dependent depletion of BRSK1 and 2 associated Tau phosphorylation (Supp Fig
416 2e-f). Importantly, H_2O_2-dependent loss of pTau could be reversed following exposure of
417 the cells to the physiological antioxidant glutathione (GSH) (Fig 1g). These findings
418 suggest that reversible oxidative modulation is relevant to BRSK1/2 kinase-dependent
419 signaling in human cells, which can be recapitulated *in vitro*.
420

421 **Mass spectrometric evidence that BRSK cysteine pairs can form intramolecular**
422 **disulfide bonds**
423

424 To identify residues that may contribute to redox regulation of BRSKs, we analyzed
425 tryptic peptides derived from precipitated full-length cellular BRSK1 and BRSK2 by
426 liquid chromatography–tandem mass spectrometry (LC-MS/MS). HEK-293T cells
427 transiently over-expressing Strep-tagged BRSK proteins were lysed in the presence of
428 the alkylating agent iodoacetamide to covalently block free thiol groups. LC-MS/MS
429 revealed the presence of intramolecular bonds between $C147^{BRSK1}$ - $C153^{BRSK1}$ and
430 $C191^{BRSK1}$ - $C198^{BRSK1}$ and $C132^{BRSK2}$ - $C138^{BRSK2}$ and $C176^{BRSK2}$ - $C183^{BRSK2}$ (Fig 2a).
431 Of note, all identified disulfide forming Cys residues were located in the kinase domains
432 of the two proteins, in close proximity to known catalytic or regulatory motifs. $C147^{BRSK1}$
433 - $C153^{BRSK1}$ and $C132^{BRSK2}$ - $C138^{BRSK2}$ structurally link the HRD motif in the catalytic
434 loop to the preceding E-helix, and $C191^{BRSK1}$ - $C198^{BRSK1}$ and $C176^{BRSK2}$ - $C183^{BRSK2}$
435 couple the T-loop Cys to the Cys residue of the CPE motif in BRSK1/2 (equivalent to the
436 APE motif in most kinase activation segments) (Fig 2b). To study these reactive Cys
437 residues in the context of catalysis, we purified the unphosphorylated catalytic domain
438 of human $BRSK1^{29-358}$ (BRSK1cat) or $BRSK2^{14-341}$ (BRSK2cat) to homogeneity from *E.*
439 *coli*. As expected, both truncated variants of BRSK were completely inactivate in our
440 AMARA-based kinase assay, but could be 'switched on' following incubation with the
441 physiological upstream regulator LKB1 (Fig 2c). Of note, despite sharing ~95%
442 sequence identity within their kinase domain, LKB1-activated BRSK2 had higher
443 catalytic activity compared to BRSK1 (Fig 2c). Moreover, and in support of our previous
444 findings for full-length BRSK proteins (Fig1), incubation of LKB1-activated WT BRSK1
445 or 2 with DTT greatly increased activity (Fig 2c). These data are consistent with

446 regulatory Cys-based modification of the kinase domain under oxidative conditions,
447 which can be reversed with a reducing agent *in vitro*.
448
449 **Emergence and structural location of cysteines residues in BRSK proteins**
450 Reversible redox regulation of signaling proteins typically requires sulfenyl derivatization
451 of an exposed Cys residue(s) (Heppner, Janssen-Heininger, and van der Vliet 2017).
452 Cys is the second least abundant amino acid in the vertebrate proteome, and conserved
453 surface exposed Cys side chains can function as redox "hotspots" (Fomenko, Marino,
454 and Gladyshev 2008; Su et al. 2019; Xiao et al. 2020). Previously, we established that
455 all 14 members of the ARK family kinases, including BRSK1 and 2, contain a T-loop + 2
456 Cys residue. This residue is equivalent to the redox sensitive C199 found in PKA
457 (Humphries, Juliano, and Taylor 2002) and is prognostic of redox regulation for multiple
458 human Ser/Thr kinases (Byrne et al., 2020). Of the ARK family kinases that we
459 previously analyzed, AMPKα1, SIK1-3 and MELK were all acutely inhibited by H_2O_2 in a
460 reversible manner *in vitro*, which we attributed to sulfenylation of the activation segment
461 Cys, based on biochemical and evolutionary analysis (Byrne et al., 2020). The T-loop +
462 2 Cys corresponds to $C191^{BRSK1}$ and $C176^{BRSK2}$ in BRSK1 and 2 respectively. This
463 residue is located within the canonical activation segment, in close proximity to the
464 regulatory site of LKB1 phosphorylation. Interestingly, mapping of Cys residues across
465 the human ARK family reveals several conserved Cys located throughout their kinase
466 domains (Fig 3a and b). However, these studies also reveal a distinguishing Cys
467 residue that is unique to the catalytic domain of human BRSKs, which is located at the
468 canonical alanine position of the "APE" motif, converting it to "CPE" ($C198^{BRSK1}$/
469 $C183^{BRSK2}$ (Fig 3b). Of note, the unusual CPE Cys forms an intramolecular disulfide with
470 the T-loop +2 Cys (Fig 2a). Intramolecular dimers incorporating T-loop Cys have also
471 been identified in MELK and AKT2 (Cao et al. 2013; Huang et al. 2003). MELK is
472 exceptional in that it possesses both a T-loop +1 as well as a T-loop +2 Cys, where the
473 T-loop +1 Cys forms an intramolecular disulfide with a Cys proximal to the DFG motif
474 and the T-loop +2 can form an intermolecular disulfide potentiating dimerization (Cao et
475 al. 2013). In the case of AKT2, the T-loop +2 Cys forms an intramolecular disulfide with
476 a Cys equivalent to that seen in MELK (Huang et al. 2003). In addition to the T+2 Cys,

477 most human ARK family members (with the exception of MELK) contain an additional
478 conserved Cys positioned 7 residues upstream of the HRD motif (HRD -7 Cys) located
479 in the E-helix (Fig 3a and b). BRSKs share the HRD -7 Cys ($C147^{BRSK1}$/ $C132^{BRSK2}$), but
480 further diverge from other ARK family members with the insertion of an additional
481 potential disulfide bond-forming Cys residues preceding the HRD motif in the catalytic
482 loop (CHRD-Cys, $C153^{BRSK1}$/ $C138^{BRSK2}$ in Fig 3a and b).
483
484
485 **Phylogenetic analysis of BRSK protein sequences**
486 A sequence-based analysis reveals the emergence of an early BRSK1 variant, which
487 we term 'proto-BRSK1' that distinguishes it from the closely related AMPKs (Supp Fig
488 1a). This is followed by a subsequent expansion of BRSK1 and 2 sequences that
489 coincides with the appearance of vertebrates (Fig 3c). Sequence alignment of BRSK
490 catalytic domains from a diverse array of organisms, including the ancestral paralog and
491 invertebrate specific proto-BRSK1, confirmed general sequence similarity and tight
492 conservation of T-loop and HRD proximal Cys 'pairs' (Fig 3d). Interestingly, all BRSK
493 domains also possess a Cys residue in the N-terminal β2-β3 loop ($C54^{BRSK1}$/ $C42^{BRSK2}$),
494 and BRSK2 contains an additional residue at this site, $C39^{BRSK2}$ (Fig 3d). The
495 diversification of BRSKs from AMPKs also correlates with an increase in the total
496 number of Cys residues in the kinase domain (Supp Fig 1a). Analysis of 2805 ARK-
497 related sequences confirmed significant conservation of the T-loop + 2 and HRD -7 Cys,
498 which were found respectively in ~18 % and ~10 % of ePKs across diverse eukaryotic
499 species (Fig 3e). These Cys residues were invariant in vertebrate BRSK sequences, as
500 were the BRSK specific CPE and HRD -1 Cys residues (Fig 3e). Unsurprisingly,
501 substitution of the APE Ala (PKA position 206, found in ~65 % of ePKs) with a Cys is
502 extremely uncommon (~1 %) in nearly all protein kinases, given the critical role of this
503 motif in stabilizing the C-lobe and substrate interactions (Supp Fig 1b). The distribution
504 of amino acids at HRD -1 position is much more variable in ePKs, with Ile and Val being
505 most commonly conserved (~36 and 30 % respectively) and a Cys appearing with
506 similar low frequency (~ 2% (Supp Fig 1b). The high degree of conservation observed
507 for these Cys residues within vertebrate BRSKs indicates that they play critical

508 functional or structural roles in these kinases (Fig 3e). This further suggests that
509 diversification of the BRSKs in metazoans correlated with the accumulation of close
510 proximity Cys 'pairs' with the potential to form regulatory disulfide bonds.
511
512 **Cysteine residues within the kinase domain fine-tune BRSK activity**
513 To assess the role of BRSK domain Cys residues in modulating catalytic activity, we
514 expressed and purified wild-type (WT) and Cys-to-Ala variants of the BRSK1 and 2
515 kinase domains in *E. coli*. These Cys-to-Ala variants included T-loop +2 Cys mutants
516 (C191A^{BRSK1} and C176A^{BRSK2}), and T-loop CPE mutants (C198A^{BRSK1} and C183A^{BRSK2}),
517 expressed either in a WT or mutant T-loop +2 Cys background (C191/198A^{BRSK1} and
518 C176/183A^{BRSK2}). We also generated double mutants of the Cys residues upstream of
519 the HRD motif (C147/153A^{BRSK1} and BRSK2 C132/138A^{BRSK2}), and the unique N-
520 terminal Cys pair in BRSK2 (C39/42A^{BRSK2}). All recombinant BRSK proteins were
521 expressed in *E. coli* and purified without DTT. Crucially, we were able to detect
522 intramolecular disulfide bonds (C191^{BRSK1} - C198^{BRSK1} and C176^{BRSK2} - C183^{BRSK2}) in
523 the WT proteins by LC-MS/MS (Supp Fig 3). Interestingly, we could only identify an
524 HRD proximal disulfide bond (C147^{BRSK1} - C153^{BRSK1}) in BRSK1 under these specific
525 experimental conditions (Supp Fig 3). We next probed for mixed disulfide formation in
526 the presence of glutathione, using an antibody that recognizes glutathionylated proteins.
527 We detected robust glutathionylation of both BRSK1 and BRSK2 in the presence of
528 either reduced (GSH) or oxidized (GSSG) glutathione, and the signal strength inversely
529 correlated with the presence of DTT (Supp Fig 4a). Of note, all of the BRSK Cys-to-Ala
530 mutants studied here could be readily glutathionylated, which supports the existence of
531 multiple reactive Cys residues within the kinase domains of BRSK1 and 2. To detect
532 alterations in redox regulation, all BRSK proteins were first activated by incubation with
533 LKB1, and T-loop phosphorylation was confirmed by immunoblotting (Supp Fig 4b). The
534 active BRSK1/2 kinases were then assayed using the specific AMARA peptide in the
535 presence or absence of fixed concentrations of DTT, and kinase activity was normalized
536 to pBRSK signal derived from Supp Fig 4b. In agreement with our previous findings with
537 full-length BRSKs, DTT was strongly activating for WT variants of both kinases, and this
538 effect was severely blunted for the T-loop +2 Cys-Ala mutants, which exhibited lower

539 basal rates of peptide phosphorylation. This is entirely consistent with our previous
540 observations for Cys-based mutants of analogous residues in a range of distinct Ser/Thr
541 kinases (Byrne et al. 2020) (Fig 4a and b). Of note, despite sharing ~95% sequence
542 identity within their kinase domain, LKB1-activated BRSK2 demonstrated enhanced
543 catalytic activity compared to BRSK1 (Fig 4b compared to a). Perhaps unsurprisingly,
544 given their distant location on an N-lobe loop, mutation of the BRSK2 exclusive
545 $C39^{BRSK2}$ and $C42^{BRSK2}$ residues had limited effect on the activity of BRSK2 (Fig 4b). In
546 contrast, tandem mutation of the HRD proximal Cys residues resulted in pronounced
547 abrogation of kinase activity, regardless of assay conditions for both kinases (Fig 4a and
548 b). Given the near absolute conservation of the HRD -7 Cys in the ARK family of protein
549 kinases, it is possible that this residue ($C147^{BRSK1}$ and $C132^{BRSK2}$) is functionally
550 important for catalytic activity in some yet unidentified capacity. Interestingly, mutation of
551 the CPE motif Cys (T-loop +9 Cys), and *de facto* restoration of the canonical APE motif,
552 were insufficient to blunt DTT-dependent activation of either kinase. Moreover, this
553 mutation, which would eliminate $C191^{BRSK1}$ - $C198^{BRSK1}$ and $C176^{BRSK2}$ - $C183^{BRSK2}$
554 disulfide bonds, increased basal (non-DTT stimulated) catalytic activity by 1.5-2-fold for
555 both kinases. WT forms of BRSK2, and in particular BRSK1, were strongly inhibited by
556 oxidative conditions, even when assays were preceded by DTT-dependent activation
557 (Fig 4c and d). Unsurprisingly, the low levels of detectable $C191A^{BRSK1}$ and $C176A^{BRSK2}$
558 activity that could be measured following stimulation by DTT were completely abolished
559 following the addition of H_2O_2. In contrast, CPE mutants ($C198A^{BRSK1}$ and $C183A^{BRSK2}$)
560 were sharply activated by DTT but still exhibited further oxidative inhibition (Fig 4c and
561 d), although to a lesser extent than their WT counterparts, particularly in the case of
562 BRSK1.
563 To ensure that the observed variations in activity between variants of BRSK1/2 were not
564 a consequence of structural impairment, we also performed differential scanning
565 fluorometry (DSF) to assess protein folding and stability. Incubation of WT BRSK1 and 2
566 with DTT had no measurable effect on the thermal stability of either protein, suggesting
567 that chemical disruption of pre-formed disulfide bonds had a minimal detectable impact
568 on global protein stability, despite greatly increasing kinase activity (Supp Fig 4c). These
569 assays also revealed only minor perturbations in protein thermal stability due to the

incorporation of specified Cys-to-Ala mutants. Interestingly, we observed a consistent decrease in T_m values for C147/153A^{BRSK1} and C132/138A^{BRSK2} (ΔT_m ~ -2 °C), suggesting a modest decrease in protein stability, and increased T_m values for CPE mutants (C198A^{BRSK1} and C183A^{BRSK2}; ΔT_m ~ +3 °C) (Supp Fig 4d).

Cellular analysis of BRSK Cys-based regulation

We next evaluated the relative contributions of the conserved T-loop Cys residues to BRSK redox sensitivity in a cellular context using our EGFP-Tau HEK-293T co-expression system and full length BRSK proteins. Mirroring our peptide-based kinase assays, loss of the T-loop +2 Cys residue evoked a marked decrease in BRSK-dependent Tau phosphorylation **(**Fig 5a and 5b**).** In contrast, mutation of the CPE Cys to an alanine consistently increased overall Tau phosphorylation (~1.5 and ~1.2 fold increase relative to WT BRSK1 and BRSK2 respectively) (Fig 5). Interestingly, the CPE mutations preserved BRSK redox sensitivity in cells treated with hydrogen peroxide, and inclusion of GSH was sufficient to restore BRSK-dependent pTau signals. Finally, we extended our analysis to consider the BRSK1 and 2 HRD motif proximal cysteines, and the BRSK2 exclusive C39/C42 pair. As predicted, Tau phosphorylation by BRSK2 C39/42A (which closely matched the activity profile of WT BRSK2 in our *in vitro* kinase assays (Fig 4)) was comparable to that observed for WT (but still less than hyper-active BRSK2 C183A) and was also similarly inhibited by the presence of H_2O_2 (Supp Fig 4e). Using the AMARA peptide as a substrate, we previously demonstrated that BRSK1 C147/153A and BRSK2 C132/138A were catalytically compromised (in a manner resembling the respective T-loop + 2 Cys-Ala mutants (Fig 4)). It is consistent that BRSK2 C132/138A was unable to increase pTau signal above background levels (Supp Fig 4e). Finally, we were unable to detect BRSK1 C147/153A protein expression in transfected cell lysates, which may indicate a loss of stability for this protein (Supp Fig 4e).

Cysteine modifications alter critical structural interactions required for kinase allosteric regulation

601 We next sought to investigate the structural basis for redox-dependent regulation of
602 BRSK activity using molecular modeling and molecular dynamics (MD) simulations. Our
603 *in vitro* analysis established that oxidative conditions inhibit the active, T-loop
604 phosphorylated form of BRSKs, and so our simulations were performed on an 'active'
605 conformation of BRSK2 generated using AlphaFold2 (see methods). Cysteine residues
606 can undergo both reversible (sulfenic) and irreversible (sulfonic) oxidation, and so
607 sulfenic acid or sulfonic acid forms of Cys were incorporated at the C176^{BRSK2} and
608 C183^{BRSK2} positions. Additionally, the impact of a non-redox active 'silent' Ala residue
609 was also modelled at these sites.
610 The T+2 C176^{BRSK2} is in close proximity to threonine T174^{BRSK2}, phosphorylation of
611 which stabilizes the kinase domain in an active conformation through salt bridge
612 interactions with charged residues in the catalytic loop (Fig 6a). In particular, R140^{BRSK2}
613 in the canonical HRD motif coordinates with the phosphate group of pT174^{BRSK2} (Nolen,
614 Taylor, and Ghosh 2004). Simulations demonstrate that the R140^{BRSK2}-pT174^{BRSK2} salt
615 bridge is preserved across the entire MD simulation, as demonstrated by the contact
616 map (Fig 6b). In the C176Ala^{BRSK2} simulations, the coordination between R140^{BRSK2} and
617 pT174^{BRSK2} is partially attenuated due to an increase in the flexibility of pT174^{BRSK2} (Fig
618 6c). This predicted increase in flexibility may explain the loss of BRSK2 catalytic activity
619 for C176A^{BRSK2} mutant (Fig 4). However, oxidative modification of C176^{BRSK2} did not
620 result in a substantial disruption of the salt bridge interaction (Fig 6d,e). As such, it is
621 unclear at this stage precisely how oxidation of the T+2 Cys exerts is regulatory effect
622 on BRSK2 kinase activity.
623 In contrast to C176^{BRSK2}, C183^{BRSK2} within the CPE motif is buried in the C-terminal lobe
624 of the kinase domain, and the SH group of C183^{BRSK2} is pointed toward a canonical salt
625 bridge that forms between the glutamate (E185^{BRSK2}) in the APE/CPE motif and
626 R259^{BRSK2} in the I-helix (Fig 6f). The E185-R259 salt bridge is a eukaryotic protein
627 kinase (EPK)-specific interaction that is critical for maintaining the EPK fold and for
628 allosterically coupling the T-Loop to distal substrate binding and regulatory sites (Yang
629 et al. 2012; Oruganty and Kannan 2012). The selective conservation of Cys in place of
630 Ala in the APE motif represents an interesting divergence of BRSKs from other ARK
631 family kinases (Fig 3e, Supp fig 1). When C183^{BRSK2} is in a reduced form or mutated to

632 an alanine, the E185-R259 is maintained throughout the MD simulation (Fig 6g/i)
633 Remarkably, in simulations incorporating oxidative modification of C183^{BRSK2} we
634 observed the immediate breaking of the E185-R259 salt bridge, and this contact
635 remains broken throughout the simulation (Fig 6h,j). Oxidation of C183^{BRSK2} to either
636 sulfenic or sulfonic acid rewires this salt bridge, with R259^{BRSK2} exclusively interacting
637 with the oxidized C183^{BRSK2} while E185^{BRSK2} pivots outward and becomes more solvent-
638 exposed. Thus, oxidized C183^{BRSK2} mediated disruption of E185-R259 ^{BRSK2} salt bridge
639 represents a unique inactive state in BRSKs which breaks the allosteric network that
640 allows cross-communication between the T-loop and the C-Lobe.
641 Surprisingly, simulations incorporating intramolecular disulfide bonds identified in
642 MS/MS experiments did not indicate any major changes in dynamics resulting from
643 either the Cys132-138 or the Cys176-183 disulfide bond formation. Most of the
644 fluctuations in these simulations were confined to the G-Loop and β3-αC loop, which
645 are distal from the disulfide bonds (Supp. Fig 5)
646
647 **Recombinant BRSK proteins form limited protein dimers**
648 Several ARK family members form disulfide bond-dependent dimers (Nayak et al. 2006;
649 Marx et al. 2010; Cao et al. 2013). To evaluate the formation of intermolecular
650 disulfides, we subjected purified kinase domains of BRSK1 and 2 isolated from *E. coli* to
651 non-reducing SDS-PAGE, followed by western blotting to probe for higher order BRSK
652 structures (Fig 7). This revealed multiple species of each kinases possessing drastically
653 decreased electrophoretic mobility compared to the major BRSK1/2 monomer bands.
654 These species increased in abundance in the presence of H_2O_2 and were absent when
655 DTT was included. Of particular significance was the appearance of a prominent
656 oxidation-dependent species at ~70 kDa, the approximate molecular weight of a BRSK
657 dimer. Consistently, all higher molecular weight species resolved into a single monomer
658 band after reducing (+DTT) SDS-PAGE, which strongly implicates disulfide bond-
659 dependent oligomerization. Curiously, mutation of the T+2 Cys had no discernable
660 effect on the formation of BRSK oligomers, although this is consistent with our previous
661 observation of multiple reactive Cys residues in BRSKs that may be capable of forming
662 a broad variety of intermolecular disulfide bonds. However, it is noteworthy that even in

663 the presence of peroxide, the majority of the BRSK1 and 2 proteins existed as a
664 monomeric species, which suggests that oligomerization is unlikely to be the primary
665 driver of oxidative inhibition that we detect in kinase-based peptide assays.
666 Furthermore, we detected interactions between BRSK1 and BRSK2 (suggesting homo-
667 and heterodimer formation) after co-immunoprecipitation of alternatively tagged variants
668 of the full length proteins overexpressed in the HEK-293T system (Supp Fig 6a).

669 Using SEC-MALS, we confirmed that BRSK1 and 2 (purified in the absence of DTT)
670 were near-uniformly monomeric in solution, but possessed the potential to self-
671 associate and form dimers. The molar mass points across the monomer peak indicates
672 a high degree of homogeneity (weight-average molar mass M_w = ~42 kDa ± 0.99 % and
673 ~43 kDa ± 0.25 %, respectively Supp Fig 6b and c). Interestingly, the BRSK2 spectra
674 included a high molecular weight shoulder of an approximate dimer size (M_w = ~75 kDa
675 ± 2.1 %) that exhibited non-uniform molar mass points indicative of a heterogenous
676 population (likely as a consequence of poor separation between the two peaks and
677 higher order oligomers). SEC-MALS also confirmed the presence of a BRSK species of
678 approximate dimer size (M_w = ~80 kDa) for $C183^{BRSK2}$ that was noticeably absent for
679 $C176^{BRSK2}$ (Supp Fig 6d and e). Although the major species observed for both mutants
680 was a monomer, the inability to detect dimer-like peaks for $C176^{BRSK2}$ may suggest that
681 the T-+2 Cys plays a role in dimerisation. Although we have searched for BRSK1/2
682 inter-molecular disulfide bonds in our LC-MS/MS data in an attempt to characterize the
683 mechanism of dimer formation, we were unable to identify any inter-molecular linked
684 peptides. This is likely due to the extremely low abundance of these dimeric species in
685 this sample (thus yielding a very small proportion of inter-linked tryptic peptides) and/or
686 because inter-molecular disulfide linked tryptic peptides are too large for identification
687 using this analytical pipeline. Collectively these findings confirm that the isolated kinase
688 domains of both BRSKs primarily occupy a largely monomeric conformation and can
689 form limited higher order redox-sensitive oligomers via covalent S-S bonds *in vitro*.
690 However, although reversible oxidation-based inactivation of BRSK1 and 2 is apparent
691 in full-length BRSK1 and 2, it remains to be determined to what extent multimerization
692 modulates BRSK catalytic activity (Fig 8) or how these mechanisms might contribute to
693 signaling-based interactions in cells.

694

695 **Discussion**

696 Redox regulation of kinases and other signaling molecules is a rapidly expanding field
697 of research, which has recently extended far beyond the early observations of oxidative
698 inhibition in protein tyrosine phosphatases (Brandes, Schmitt, and Jakob 2009). More
699 recent enquiries have provided strong evidence for direct regulative oxidative
700 modification of Met and Cys residues across divergent protein kinase families, providing
701 temporal and spatial control of their catalytic outputs (Corcoran and Cotter 2013; Truong
702 and Carroll 2013; Jarvis, Hughes, and Ledgerwood 2012). However, despite the
703 prevalence of this regulatory mechanism, the structural basis to explain how redox-
704 active cysteines contribute to allosteric control of catalytic activity is largely unknown. In
705 this study, we demonstrate, for the first time, that two T-loop +2 Cys-containing
706 members of the ARK family, BRSK1 and 2, are reversibly inactivated by oxidative-
707 dependent mechanisms *in vitro* and in human cells. Moreover, we uncover a
708 multifaceted redox-activity profile for human BRSKs, involving functional Cys-pairs that
709 are conserved within the catalytic domains of these understudied enzymes. In contrast
710 to Ser/Thr kinases such as Aurora A, where a single Cys residue is the dominant driver
711 of redox-sensitivity (Byrne et al. 2020; Tsuchiya et al. 2020), BRSK1 and 2 possess
712 multiple sulfenylation-prone Cys residues. Additionally, the close proximity of distinct
713 Cys 'pairs' permits the formation of two intramolecular disulfide bonds: the first forming
714 between two HRD-motif proximal sites, and the second bridging the conserved T-loop +
715 2 and unique 'CPE' motif Cys residues. We propose a model where disulfide bond
716 formation can impose a steric block on kinase activity whilst structural perturbations,
717 likely emanating from sulfenylation of conserved BRSK family Cys residues within
718 critical kinase regulatory motifs, provides an additional layer of tunable regulation
719 Validation of these reversibly oxidized Cys species is also of relevance as this may
720 implicate a mechanistic role for ROS sensing in the largely obscure BRSK signaling
721 pathways that operate in different cell types, including those that impact on canonical
722 redox pathways that lead to NRF2 inactivation in cells (Tamir et al. 2020).

723

724 **Multilayered redox regulation of BRSKs**

725 The strategic positioning of Cys residues near key regulatory elements in the T-Loop
726 suggests an evolutionary adaptation for ROS-based sensing in protein kinases
727 (Beenstock, Mooshayef, and Engelberg 2016; Pearce, Komander, and Alessi 2010). Full
728 kinase activity typically requires T-Loop phosphorylation, a process further modulated
729 by mechanisms like allosteric activation in Aurora A (Eyers et al. 2003; Bayliss et al.
730 2003) and activation of CAMKs by CaM (Rellos et al. 2010). ARK family kinases, such
731 as BRSK1 and 2, are primed by phosphorylation in the T-loop of a single Thr residue by
732 the master regulatory kinase LKB1. However, our findings suggest that oxidation (or
733 reduction) of key reactive Cys residues in the kinase domains of BRSK1 /2 might
734 provide a 'dominant' regulatory oversight of enzyme output whose function in cells is
735 likely controlled by subcellular compartmentalization and/or partner protein interactions.
736
737 The ARK family of protein kinases (typified by AMPKα), share a conserved structure
738 with a notable conserved T-loop + 2 Cys residue, which is crucial for redox regulation,
739 as evidenced in AMPK and other ARKs (Byrne et al. 2020). Mutational analysis of the
740 T+2 Cys position in BRSKs confirms its critical role in supporting kinase activity.
741 Interestingly, a second Cys residue (HRD -7), co-conserved in most ARKs with the
742 exception of MELK, appears to add another regulatory dimension, with alanine
743 substitution at this site significantly reducing BRSK1 and 2 activity (Fig 4 and Supp Fig
744 4d3d). This is paralleled by the redox-sensitive Cys 130 in AMPK (Shao et al. 2014).
745 Moreover, the tendency of several ARKs to form disulfide bond-dependent dimers in
746 solution (Nayak et al. 2006; Marx et al. 2010; Cao et al. 2013) is corroborated by crystal
747 structures of MELK, MARK2, and BRSK2 (Fig 8b), revealing asymmetric dimers linked
748 by disulfide bridges at the T-loop + 2 Cys (Marx et al. 2010; Marx et al. 2006; Murphy et
749 al. 2007; Cao et al. 2013
750
751 **BRSK-specific adaptations relevant to Cys-based signaling?**
752 BRSKs are differentiated from other ARKs and ePKs through augmentation with two
753 unique Cys residues at the HRD -1 and T-loop +9 positions, forming a novel
754 distinguishing 'CPE' motif in place of the typical APE motif found in most human protein
755 kinases. These Cys pairs facilitate intramolecular disulfide bond formation, influencing

756 kinase activity and conformation. This mechanism is reminiscent of AKT and MELK,
757 where intramolecular disulfide bonds regulate kinase activity (Murata et al. 2003; Huang
758 et al. 2003; Byrne et al. 2020; Beullens et al. 2005). Deletion of the T-loop Cys in the
759 CPE motif partially reduces BRSK1 and 2 auto-inhibition, suggesting multiple functional
760 roles for these cysteines, which is supported by our molecular dynamics (MD)
761 simulations.
762
763 Comparative evolutionary analysis indicates that approximately 1.4% of all ePKs,
764 including AKT and MELK, have cysteines at the DFG + 2 and T-loop + 2 positions
765 capable of forming similar disulfide bridges (Byrne et al. 2020; Cao et al. 2013; Huang
766 et al. 2003). MELK, despite lacking the typical HRD -7 Cys of ARKs, has compensatory
767 activation loop Cys residues that form variable disulfide bonds (Beullens et al. 2005). A
768 broader analysis across human protein kinases shows 273 unique Cys pairs capable of
769 forming disulfide bonds, suggesting a widespread regulatory mechanism in the kinome
770 (Supp. File 1). Our findings in BRSK1 and 2 highlight an extensive intramolecular
771 disulfide network, serving as a reversible switch for kinase activity and interaction
772 regulation. When considering the dominant regulative role of the T-loop available T+2
773 Cys, it is tempting to speculate that formation of intramolecular disulfides bonds with
774 adjacent cysteines may be protective against deleterious hyper-oxidized species and
775 enable rapid re-activation of the kinase after emergence from oxidative stress conditions
776 by the disulfide reductase system (Krishnan et al. 2011; Barrett et al. 1999; Chen et al.
777 2008).
778
779 The identification and characterization of unique reactive Cys residues within the kinase
780 domains of BRSK1 and 2 reveals sites of covalent-oxidative modification that may also
781 provide an underexploited opportunity to develop targeted therapeutic strategies for
782 BRSK-associated pathologies. Furthermore, mapping the spatial distribution of Cys
783 across the AMPK-related kinase family provides valuable insights into potential redox
784 hotspots that may underpin a tunable modulation of catalytic outputs with wider
785 implications for cellular signaling. As a master regulator of metabolic homeostasis,
786 AMPK activity is central to appropriate redox balance within cells (Ren and Shen 2019;

787 Choi et al. 2001; Hawley et al. 2010; Zmijewski et al. 2010; Hinchy et al. 2018; Auciello
788 et al. 2014; Shao et al. 2014), but until recently evidence of crosstalk between BRSKs
789 and redox signaling has been less clear. However, BRSKs can indirectly modulate the
790 cellular antioxidant response by orchestrating suppression of the transcription factor
791 (and master regulator/sensor of the antioxidant response), NRF2, in an mTOR-
792 dependent manner in HEK-293 cells (Tamir et al. 2020). NRF2 is targeted for
793 proteasomal degradation by its inhibitor partner, KEAP1, and under conditions of
794 elevated ROS, oxidation of sensor Cys residues in KEAP1 allows NRF2 to escape
795 ubiquitination and induce transcription of the antioxidant machinery (Baird and
796 Yamamoto 2020). Our discovery of redox regulation in BRSKs suggests that it may be
797 part of a multi-protein Cys-based 'relay' network of ROS sensitive effectors upstream of
798 NRF2, potentially constituting a new oxidative stress signaling mechanism. Uncoupling
799 the specific role of BRSKs in this pathway will be critical in illuminating BRSK1 and 2
800 physiology and their roles in neuronal function and disease and may simultaneously
801 provide an explanation for the appearance of two functional BRSK1/2 genes in
802 vertebrates.
803

Funding and additional information

Funding from N.K. (grant no: R35 GM139656) is acknowledged. P.A.E. acknowledges funding from University of Liverpool BBSRC MRC/IAA awards. A.V. acknowledges funding from ARCS Foundation. D.P.B, L.A.D., S.O.O., P.A.E. and C.E.E. also acknowledge BBSRC grants BB/S018514/1, BB/N021703/1, BB/X002780/1 and North West Cancer Research (NWCR) grant CR1208. The content is solely the responsibility of the authors and does not necessarily represent the official views of the National Institutes of Health.

Data Availability

All data generated in this study are included within the manuscript. All mass spectrometry data has been deposited at the ProteomeXchange Consortium (http://proteomecentral.proteomexchange.org) via the PRIDE partner repository with the dataset identifiers PXD044990. Source data are provided for each figure. MD simulations and associated data may be accessed from https://www.dropbox.com/sh/xtiwpjgyzxy1oz0/AACK6dS3ypzYXDih3wgKp9bla?dl=0.

Competing Interest Statement

The authors claim no competing interest.

References

Alessi, D. R., K. Sakamoto, and J. R. Bayascas. 2006. 'LKB1-dependent signaling pathways', Annu Rev Biochem, 75: 137-63.

Askoxylakis, V., G. Millonig, U. Wirkner, C. Schwager, S. Rana, A. Altmann, U. Haberkorn, J. Debus, S. Mueller, and P. E. Huber. 2011. 'Investigation of tumor hypoxia using a two-enzyme system for in vitro generation of oxygen deficiency', Radiat. Oncol., 6: 35.

Auciello, F. R., F. A. Ross, N. Ikematsu, and D. G. Hardie. 2014. 'Oxidative stress activates AMPK in cultured cells primarily by increasing cellular AMP and/or ADP', Febs Letters, 588: 3361-6.

Baird, L., and M. Yamamoto. 2020. 'The Molecular Mechanisms Regulating the KEAP1-NRF2 Pathway', Mol Cell Biol, 40.

Barrett, W. C., J. P. DeGnore, S. Konig, H. M. Fales, Y. F. Keng, Z. Y. Zhang, M. B. Yim, and P. B. Chock. 1999. 'Regulation of PTP1B via glutathionylation of the active site cysteine 215', Biochemistry, 38: 6699-705.

Bayliss, R., T. Sardon, I. Vernos, and E. Conti. 2003. 'Structural basis of Aurora-A activation by TPX2 at the mitotic spindle', Mol Cell, 12: 851-62.

Beenstock, J., N. Mooshayef, and D. Engelberg. 2016. 'How Do Protein Kinases Take a Selfie (Autophosphorylate)?', Trends Biochem Sci, 41: 938-53.

Beullens, M., S. Vancauwenbergh, N. Morrice, R. Derua, H. Ceulemans, E. Waelkens, and M. Bollen. 2005. 'Substrate specificity and activity regulation of protein kinase MELK', J Biol Chem, 280: 40003-11.

Brandes, N., S. Schmitt, and U. Jakob. 2009. 'Thiol-based redox switches in eukaryotic proteins', Antioxid Redox Signal, 11: 997-1014.

Bright, N. J., D. Carling, and C. Thornton. 2008. 'Investigating the regulation of brain-specific kinases 1 and 2 by phosphorylation', J Biol Chem, 283: 14946-54.

Bright, N. J., C. Thornton, and D. Carling. 2009. 'The regulation and function of mammalian AMPK-related kinases', Acta Physiol (Oxf), 196: 15-26.

Brooks, B. R., C. L. Brooks, 3rd, A. D. Mackerell, Jr., L. Nilsson, R. J. Petrella, B. Roux, Y. Won, G. Archontis, C. Bartels, S. Boresch, A. Caflisch, L. Caves, Q. Cui, A. R. Dinner, M. Feig, S. Fischer, J. Gao, M. Hodoscek, W. Im, K. Kuczera, T. Lazaridis, J. Ma, V. Ovchinnikov, E. Paci, R. W. Pastor, C. B. Post, J. Z. Pu, M. Schaefer, B. Tidor, R. M. Venable, H. L. Woodcock, X. Wu, W. Yang, D. M. York, and M. Karplus. 2009. 'CHARMM: the biomolecular simulation program', Journal of Computational Chemistry, 30: 1545-614.

Byrne, D. P., S. Shrestha, M. Galler, M. Cao, L. A. Daly, A. E. Campbell, C. E. Eyers, E. A. Veal, N. Kannan, and P. A. Eyers. 2020. 'Aurora A regulation by reversible cysteine oxidation reveals evolutionarily conserved redox control of Ser/Thr protein kinase activity', Sci Signal, 13.

862 Byrne, D. P., M. Vonderach, S. Ferries, P. J. Brownridge, C. E. Eyers, and P. A. Eyers.
863 2016. 'cAMP-dependent protein kinase (PKA) complexes probed by complementary
864 differential scanning fluorimetry and ion mobility-mass spectrometry', Biochem J, 473:
865 3159-75.

866 Cao, L. S., J. Wang, Y. Chen, H. Deng, Z. X. Wang, and J. W. Wu. 2013. 'Structural
867 basis for the regulation of maternal embryonic leucine zipper kinase', PLoS One, 8:
868 e70031.

869 Cao, M., A. M. Day, M. Galler, H. R. Latimer, D. P. Byrne, T. W. Foy, E. Dwyer, E.
870 Bennett, J. Palmer, B. A. Morgan, P. A. Eyers, and E. A. Veal. 2023. 'A peroxiredoxin-
871 P38 MAPK scaffold increases MAPK activity by MAP3K-independent mechanisms', Mol
872 Cell.

873 Chen, Y. Y., H. M. Chu, K. T. Pan, C. H. Teng, D. L. Wang, A. H. Wang, K. H. Khoo,
874 and T. C. Meng. 2008. 'Cysteine S-nitrosylation protects protein-tyrosine phosphatase
875 1B against oxidation-induced permanent inactivation', J Biol Chem, 283: 35265-72.

876 Choi, S. L., S. J. Kim, K. T. Lee, J. Kim, J. Mu, M. J. Birnbaum, S. Soo Kim, and J. Ha.
877 2001. 'The regulation of AMP-activated protein kinase by H(2)O(2)', Biochem Biophys
878 Res Commun, 287: 92-7.

879 Corcoran, A., and T. G. Cotter. 2013. 'Redox regulation of protein kinases', Febs
880 Journal, 280: 1944-65.

881 Daly, L. A., P. J. Brownridge, M. Batie, S. Rocha, V. See, and C. E. Eyers. 2021.
882 'Oxygen-dependent changes in binding partners and post-translational modifications
883 regulate the abundance and activity of HIF-1alpha/2alpha', Sci Signal, 14.

884 Daly, Leonard A, Dominic P Byrne, Simon Perkins, Philip J Brownridge, Euan
885 McDonnell, Andrew R Jones, Patrick A Eyers, and Claire E Eyers. 2023. 'A bespoke
886 analytical workflow for the confident identification of sulfopeptides and their
887 discrimination from phosphopeptides', bioRxiv: 2023.07. 15.549150.

888 Deng, J., Y. Wang, M. Hu, J. Lin, Q. Li, C. Liu, and X. Xu. 2022. 'Deleterious Variation in
889 BR Serine/Threonine Kinase 2 Classified a Subtype of Autism', Front Mol Neurosci, 15:
890 904935.

891 Engh, R. A., and D. Bossemeyer. 2001. 'The protein kinase activity modulation sites:
892 mechanisms for cellular regulation - targets for therapeutic intervention', Adv Enzyme
893 Regul, 41: 121-49.

894 Eyers, P. A., E. Erikson, L. G. Chen, and J. L. Maller. 2003. 'A novel mechanism for
895 activation of the protein kinase Aurora A', Curr Biol, 13: 691-7.

896 Faezov, Bulat, and Jr. Roland L. Dunbrack. 2023. 'AlphaFold2 models of the active form
897 of all 437 catalytically-competent typical human kinase domains', bioRxiv:
898 2023.07.21.550125.

899 Ferries, S., S. Perkins, P. J. Brownridge, A. Campbell, P. A. Eyers, A. R. Jones, and C.
900 E. Eyers. 2017. 'Evaluation of Parameters for Confident Phosphorylation Site

901 Localization Using an Orbitrap Fusion Tribrid Mass Spectrometer', J Proteome Res, 16:
902 3448-59.

903 Fomenko, D. E., S. M. Marino, and V. N. Gladyshev. 2008. 'Functional diversity of
904 cysteine residues in proteins and unique features of catalytic redox-active cysteines in
905 thiol oxidoreductases', Mol Cells, 26: 228-35.

906 Forman, H. J., M. J. Davies, A. C. Kramer, G. Miotto, M. Zaccarin, H. Zhang, and F.
907 Ursini. 2017. 'Protein cysteine oxidation in redox signaling: Caveats on sulfenic acid
908 detection and quantification', Arch Biochem Biophys, 617: 26-37.

909 Foulkes, D. M., D. P. Byrne, W. Yeung, S. Shrestha, F. P. Bailey, S. Ferries, C. E.
910 Eyers, K. Keeshan, C. Wells, D. H. Drewry, W. J. Zuercher, N. Kannan, and P. A.
911 Eyers. 2018. 'Covalent inhibitors of EGFR family protein kinases induce degradation of
912 human Tribbles 2 (TRIB2) pseudokinase in cancer cells', Sci Signal, 11.

913 Garrido Ruiz, D., A. Sandoval-Perez, A. V. Rangarajan, E. L. Gunderson, and M. P.
914 Jacobson. 2022. 'Cysteine Oxidation in Proteins: Structure, Biophysics, and Simulation',
915 Biochemistry, 61: 2165-76.

916 Gupta, V., and K. S. Carroll. 2014. 'Sulfenic acid chemistry, detection and cellular
917 lifetime', Biochim Biophys Acta, 1840: 847-75.

918 Hawley, S. A., F. A. Ross, C. Chevtzoff, K. A. Green, A. Evans, S. Fogarty, M. C.
919 Towler, L. J. Brown, O. A. Ogunbayo, A. M. Evans, and D. G. Hardie. 2010. 'Use of cells
920 expressing gamma subunit variants to identify diverse mechanisms of AMPK activation',
921 Cell Metab, 11: 554-65.

922 Heppner, D. E., Y. M. W. Janssen-Heininger, and A. van der Vliet. 2017. 'The role of
923 sulfenic acids in cellular redox signaling: Reconciling chemical kinetics and molecular
924 detection strategies', Arch Biochem Biophys, 616: 40-46.

925 Hinchy, E. C., A. V. Gruszczyk, R. Willows, N. Navaratnam, A. R. Hall, G. Bates, T. P.
926 Bright, T. Krieg, D. Carling, and M. P. Murphy. 2018. 'Mitochondria-derived ROS
927 activate AMP-activated protein kinase (AMPK) indirectly', J Biol Chem, 293: 17208-17.

928 Hoang, D. T., O. Chernomor, A. von Haeseler, B. Q. Minh, and L. S. Vinh. 2018.
929 'UFBoot2: Improving the Ultrafast Bootstrap Approximation', Molecular Biology and
930 Evolution, 35: 518-22.

931 Huang, X., M. Begley, K. A. Morgenstern, Y. Gu, P. Rose, H. Zhao, and X. Zhu. 2003.
932 'Crystal structure of an inactive Akt2 kinase domain', Structure, 11: 21-30.

933 Huerta-Cepas, J., F. Serra, and P. Bork. 2016. 'ETE 3: Reconstruction, Analysis, and
934 Visualization of Phylogenomic Data', Molecular Biology and Evolution, 33: 1635-8.

935 Humphries, K. M., C. Juliano, and S. S. Taylor. 2002. 'Regulation of cAMP-dependent
936 protein kinase activity by glutathionylation', J Biol Chem, 277: 43505-11.

937 Jarvis, R. M., S. M. Hughes, and E. C. Ledgerwood. 2012. 'Peroxiredoxin 1 functions as
938 a signal peroxidase to receive, transduce, and transmit peroxide signals in mammalian
939 cells', Free Radic Biol Med, 53: 1522-30.

940 Jo, S., X. Cheng, S. M. Islam, L. Huang, H. Rui, A. Zhu, H. S. Lee, Y. Qi, W. Han, K.
941 Vanommeslaeghe, A. D. MacKerell, Jr., B. Roux, and W. Im. 2014. 'CHARMM-GUI PDB
942 manipulator for advanced modeling and simulations of proteins containing nonstandard
943 residues', Adv Protein Chem Struct Biol, 96: 235-65.

944 Jumper, J., R. Evans, A. Pritzel, T. Green, M. Figurnov, O. Ronneberger, K.
945 Tunyasuvunakool, R. Bates, A. Zidek, A. Potapenko, A. Bridgland, C. Meyer, S. A. A.
946 Kohl, A. J. Ballard, A. Cowie, B. Romera-Paredes, S. Nikolov, R. Jain, J. Adler, T. Back,
947 S. Petersen, D. Reiman, E. Clancy, M. Zielinski, M. Steinegger, M. Pacholska, T.
948 Berghammer, S. Bodenstein, D. Silver, O. Vinyals, A. W. Senior, K. Kavukcuoglu, P.
949 Kohli, and D. Hassabis. 2021. 'Highly accurate protein structure prediction with
950 AlphaFold', Nature, 596: 583-89.

951 Kalyaanamoorthy, S., B. Q. Minh, T. K. F. Wong, A. von Haeseler, and L. S. Jermiin.
952 2017. 'ModelFinder: fast model selection for accurate phylogenetic estimates', Nat
953 Methods, 14: 587-89.

954 Kishi, M., Y. A. Pan, J. G. Crump, and J. R. Sanes. 2005. 'Mammalian SAD kinases are
955 required for neuronal polarization', Science, 307: 929-32.

956 Krishnan, N., C. Fu, D. J. Pappin, and N. K. Tonks. 2011. 'H2S-Induced sulfhydration of
957 the phosphatase PTP1B and its role in the endoplasmic reticulum stress response', Sci
958 Signal, 4: ra86.

959 Lee, J., X. Cheng, J. M. Swails, M. S. Yeom, P. K. Eastman, J. A. Lemkul, S. Wei, J.
960 Buckner, J. C. Jeong, Y. Qi, S. Jo, V. S. Pande, D. A. Case, C. L. Brooks, 3rd, A. D.
961 MacKerell, Jr., J. B. Klauda, and W. Im. 2016. 'CHARMM-GUI Input Generator for
962 NAMD, GROMACS, AMBER, OpenMM, and CHARMM/OpenMM Simulations Using the
963 CHARMM36 Additive Force Field', J Chem Theory Comput, 12: 405-13.

964 Lennicke, C., J. Rahn, R. Lichtenfels, L. A. Wessjohann, and B. Seliger. 2015.
965 'Hydrogen peroxide - production, fate and role in redox signaling of tumor cells', Cell
966 Commun Signal, 13: 39.

967 Li, R., M. He, B. Wu, P. Zhang, Q. Zhang, and Y. Chen. 2020. 'SAD-B modulates
968 epileptic seizure by regulating AMPA receptors in patients with temporal lobe epilepsy
969 and in the PTZ-induced epileptic model', Braz J Med Biol Res, 53: e9175.

970 Lizcano, J. M., O. Goransson, R. Toth, M. Deak, N. A. Morrice, J. Boudeau, S. A.
971 Hawley, L. Udd, T. P. Makela, D. G. Hardie, and D. R. Alessi. 2004. 'LKB1 is a master
972 kinase that activates 13 kinases of the AMPK subfamily, including MARK/PAR-1',
973 EMBO J, 23: 833-43.

974 Manning, G., D. B. Whyte, R. Martinez, T. Hunter, and S. Sudarsanam. 2002. 'The
975 protein kinase complement of the human genome', Science, 298: 1912-34.

976 Marx, A., C. Nugoor, J. Muller, S. Panneerselvam, T. Timm, M. Bilang, E. Mylonas, D. I.
977 Svergun, E. M. Mandelkow, and E. Mandelkow. 2006. 'Structural variations in the
978 catalytic and ubiquitin-associated domains of microtubule-associated
979 protein/microtubule affinity regulating kinase (MARK) 1 and MARK2', J Biol Chem, 281:
980 27586-99.

981 Marx, A., C. Nugoor, S. Panneerselvam, and E. Mandelkow. 2010. 'Structure and
982 function of polarity-inducing kinase family MARK/Par-1 within the branch of AMPK/Snf1-
983 related kinases', FASEB J, 24: 1637-48.

984 Michaud-Agrawal, N., E. J. Denning, T. B. Woolf, and O. Beckstein. 2011. 'MDAnalysis:
985 a toolkit for the analysis of molecular dynamics simulations', Journal of Computational
986 Chemistry, 32: 2319-27.

987 Minh, B. Q., H. A. Schmidt, O. Chernomor, D. Schrempf, M. D. Woodhams, A. von
988 Haeseler, and R. Lanfear. 2020. 'IQ-TREE 2: New Models and Efficient Methods for
989 Phylogenetic Inference in the Genomic Era', Molecular Biology and Evolution, 37: 1530-
990 34.

991 Mohanty, S., K. Oruganty, A. Kwon, D. P. Byrne, S. Ferries, Z. Ruan, L. E. Hanold, S.
992 Katiyar, E. J. Kennedy, P. A. Eyers, and N. Kannan. 2016. 'Hydrophobic Core Variations
993 Provide a Structural Framework for Tyrosine Kinase Evolution and Functional
994 Specialization', PLoS Genet, 12: e1005885.

995 Morshed, Nader, Meelim J Lee, Felicia H Rodriguez, Douglas A Lauffenburger, Diego
996 Mastroeni, and Forest M White. 2021. 'Quantitative phosphoproteomics uncovers
997 dysregulated kinase networks in Alzheimer's disease', Nature Aging, 1: 550-65.

998 Mueller, S., G. Millonig, and G. Waite. 2009. 'The GOX/CAT system: A novel enzymatic
999 method to independently control hydrogen peroxide and hypoxia in cell culture', Adv.
1000 Med. Sci., 54: 121–135.

1001 Murata, H., Y. Ihara, H. Nakamura, J. Yodoi, K. Sumikawa, and T. Kondo. 2003.
1002 'Glutaredoxin exerts an antiapoptotic effect by regulating the redox state of Akt', J Biol
1003 Chem, 278: 50226-33.

1004 Murphy, J. M., D. M. Korzhnev, D. F. Ceccarelli, D. J. Briant, A. Zarrine-Afsar, F.
1005 Sicheri, L. E. Kay, and T. Pawson. 2007. 'Conformational instability of the MARK3 UBA
1006 domain compromises ubiquitin recognition and promotes interaction with the adjacent
1007 kinase domain', Proc Natl Acad Sci U S A, 104: 14336-41.

1008 Murphy, J. M., Q. Zhang, S. N. Young, M. L. Reese, F. P. Bailey, P. A. Eyers, D.
1009 Ungureanu, H. Hammaren, O. Silvennoinen, L. N. Varghese, K. Chen, A. Tripaydonis,
1010 N. Jura, K. Fukuda, J. Qin, Z. Nimchuk, M. B. Mudgett, S. Elowe, C. L. Gee, L. Liu, R. J.
1011 Daly, G. Manning, J. J. Babon, and I. S. Lucet. 2014. 'A robust methodology to
1012 subclassify pseudokinases based on their nucleotide-binding properties', Biochem J,
1013 457: 323-34.

1014 Nayak, V., K. Zhao, A. Wyce, M. F. Schwartz, W. S. Lo, S. L. Berger, and R.
1015 Marmorstein. 2006. 'Structure and dimerization of the kinase domain from yeast Snf1, a
1016 member of the Snf1/AMPK protein family', Structure, 14: 477-85.

1017 Nakanishi, K., H. Niida, H. Tabata, T. Ito, Y. Hori, M. Hattori, Y. Johmura, C. Yamada, T.
1018 Ueda, K. Takeuchi, K. Yamada, K. Nagata, N. Wakamatsu, M. Kishi, Y. A. Pan, S.
1019 Ugawa, S. Shimada, J. R. Sanes, Y. Higashi, and M. Nakanishi. 2019. 'Isozyme-
1020 Specific Role of SAD-A in Neuronal Migration During Development of Cerebral Cortex',
1021 Cerebral Cortex, 29: 3738-51.

1022 Nayak, V., K. Zhao, A. Wyce, M. F. Schwartz, W. S. Lo, S. L. Berger, and R.
1023 Marmorstein. 2006. 'Structure and dimerization of the kinase domain from yeast Snf1, a
1024 member of the Snf1/AMPK protein family', Structure, 14: 477-85.

1025 Neuwald, A. F. 2009. 'Rapid detection, classification and accurate alignment of up to a
1026 million or more related protein sequences', Bioinformatics, 25: 1869-75.

1027 Nie, J., C. Sun, O. Faruque, G. Ye, J. Li, Q. Liang, Z. Chang, W. Yang, X. Han, and Y.
1028 Shi. 2012. 'Synapses of amphids defective (SAD-A) kinase promotes glucose-
1029 stimulated insulin secretion through activation of p21-activated kinase (PAK1) in
1030 pancreatic beta-Cells', J Biol Chem, 287: 26435-44.

1031 Nolen, B., S. Taylor, and G. Ghosh. 2004. 'Regulation of protein kinases; controlling
1032 activity through activation segment conformation', Mol Cell, 15: 661-75.

1033 Pearce, L. R., D. Komander, and D. R. Alessi. 2010. 'The nuts and bolts of AGC protein
1034 kinases', Nat Rev Mol Cell Biol, 11: 9-22.

1035 Perkins, D. N., D. J. Pappin, D. M. Creasy, and J. S. Cottrell. 1999. 'Probability-based
1036 protein identification by searching sequence databases using mass spectrometry data',
1037 Electrophoresis, 20: 3551-67.

1038 Poole, L. B. 2015. 'The basics of thiols and cysteines in redox biology and chemistry',
1039 Free Radic Biol Med, 80: 148-57.

1040 Rellos, P., A. C. Pike, F. H. Niesen, E. Salah, W. H. Lee, F. von Delft, and S. Knapp.
1041 2010. 'Structure of the CaMKIIdelta/calmodulin complex reveals the molecular
1042 mechanism of CaMKII kinase activation', PLoS Biol, 8: e1000426.

1043 Ren, Y., and H. M. Shen. 2019. 'Critical role of AMPK in redox regulation under glucose
1044 starvation', Redox Biol, 25: 101154.

1045 Rhee, S. G., S. W. Kang, W. Jeong, T. S. Chang, K. S. Yang, and H. A. Woo. 2005.
1046 'Intracellular messenger function of hydrogen peroxide and its regulation by
1047 peroxiredoxins', Curr Opin Cell Biol, 17: 183-9.

1048 Saiyin, H., N. Na, X. Han, Y. Fang, Y. Wu, W. Lou, and X. Yang. 2017. 'BRSK2 induced
1049 by nutrient deprivation promotes Akt activity in pancreatic cancer via downregulation of
1050 mTOR activity', Oncotarget, 8: 44669-81.

1051 Salmeen, A., J. N. Andersen, M. P. Myers, T. C. Meng, J. A. Hinks, N. K. Tonks, and D.
1052 Barford. 2003. 'Redox regulation of protein tyrosine phosphatase 1B involves a
1053 sulphenyl-amide intermediate', Nature, 423: 769-73.

1054 Schieber, M., and N. S. Chandel. 2014. 'ROS function in redox signaling and oxidative
1055 stress', Curr Biol, 24: R453-62.

1056 Schrodinger, LLC. 2015. "The PyMOL Molecular Graphics System, Version 1.8." In.

1057 Shao, D., S. Oka, T. Liu, P. Zhai, T. Ago, S. Sciarretta, H. Li, and J. Sadoshima. 2014.
1058 'A redox-dependent mechanism for regulation of AMPK activation by Thioredoxin1
1059 during energy starvation', Cell Metab, 19: 232-45.

1060 Shirwany, N. A., and M. H. Zou. 2014. 'AMPK: a cellular metabolic and redox sensor. A
1061 minireview', Front Biosci (Landmark Ed), 19: 447-74.

1062 Soylu, I., and S. M. Marino. 2016. 'Cy-preds: An algorithm and a web service for the
1063 analysis and prediction of cysteine reactivity', Proteins, 84: 278-91.

1064 Su, Z., J. G. Burchfield, P. Yang, S. J. Humphrey, G. Yang, D. Francis, S. Yasmin, S. Y.
1065 Shin, D. M. Norris, A. L. Kearney, M. A. Astore, J. Scavuzzo, K. H. Fisher-Wellman, Q.
1066 P. Wang, B. L. Parker, G. G. Neely, F. Vafaee, J. Chiu, R. Yeo, P. J. Hogg, D. J.
1067 Fazakerley, L. K. Nguyen, S. Kuyucak, and D. E. James. 2019. 'Global redox proteome
1068 and phosphoproteome analysis reveals redox switch in Akt', Nat Commun, 10: 5486.

1069 Tamir, T. Y., D. H. Drewry, C. Wells, M. B. Major, and A. D. Axtman. 2020. 'PKIS deep
1070 dive yields a chemical starting point for dark kinases and a cell active BRSK2 inhibitor',
1071 Sci Rep, 10: 15826.

1072 Tamir, T. Y., B. M. Bowman, M. J. Agajanian, D. Goldfarb, T. P. Schrank, T. Stohrer, A.
1073 E. Hale, P. F. Siesser, S. J. Weir, R. M. Murphy, K. M. LaPak, B. E. Weissman, N. J.
1074 Moorman, and M. B. Major. 2020. 'Gain-of-function genetic screen of the kinome
1075 reveals BRSK2 as an inhibitor of the NRF2 transcription factor', J Cell Sci, 133.

1076 Truong, T. H., and K. S. Carroll. 2013. 'Redox regulation of protein kinases', Crit Rev
1077 Biochem Mol Biol, 48: 332-56.

1078 Truong, T. H., P. M.-U. Ung, P. B. Palde, C. E. Paulsen, A. Schlessinger, and K. S.
1079 Carroll. 2016. 'Molecular basis for redox activation of epidermal growth factor receptor
1080 kinase', Cell Chem. Biol., 23: 837–848.

1081 Tsuchiya, Y., D. P. Byrne, S. G. Burgess, J. Bormann, J. Bakovic, Y. Huang, A.
1082 Zhyvoloup, B. Y. K. Yu, S. Peak-Chew, T. Tran, F. Bellany, A. B. Tabor, A. E. Chan, L.
1083 Guruprasad, O. Garifulin, V. Filonenko, M. Vonderach, S. Ferries, C. E. Eyers, J.
1084 Carroll, M. Skehel, R. Bayliss, P. A. Eyers, and I. Gout. 2020. 'Covalent Aurora A
1085 regulation by the metabolic integrator coenzyme A', Redox Biol, 28: 101318.

1086 UniProt, Consortium. 2023. 'UniProt: the Universal Protein Knowledgebase in 2023',
1087 Nucleic Acids Res, 51: D523-D31.

1088 Van Der Spoel, D., E. Lindahl, B. Hess, G. Groenhof, A. E. Mark, and H. J. Berendsen.
1089 2005. 'GROMACS: fast, flexible, and free', Journal of Computational Chemistry, 26:
1090 1701-18.

1091 van Montfort, R. L., M. Congreve, D. Tisi, R. Carr, and H. Jhoti. 2003. 'Oxidation state of
1092 the active-site cysteine in protein tyrosine phosphatase 1B', Nature, 423: 773-7.

1093 Venkat, A., G. Watterson, D. P. Byrne, B. O'Boyle, S. Shrestha, N. Gravel, E. E.
1094 Fairweather, L. A. Daly, C. Bunn, W. Yeung, I. Aggarwal, S. Katiyar, C. E. Eyers, P. A.
1095 Eyers, and N. Kannan. 2023. 'Mechanistic and evolutionary insights into isoform-specific
1096 'supercharging' in DCLK family kinases', bioRxiv.

1097 Wani, R., J. Qian, L. Yin, E. Bechtold, S. B. King, L. B. Poole, E. Paek, A. W. Tsang,
1098 and C. M. Furdui. 2011. 'Isoform-specific regulation of Akt by PDGF-induced reactive
1099 oxygen species', Proc Natl Acad Sci U S A, 108: 10550-5.

1100 Weisner, J., R. Gontla, L. van der Westhuizen, S. Oeck, J. Ketzer, P. Janning, A.
1101 Richters, T. Muhlenberg, Z. Fang, A. Taher, V. Jendrossek, S. C. Pelly, S. Bauer, W. A.
1102 van Otterlo, and D. Rauh. 2015. 'Covalent-Allosteric Kinase Inhibitors', Angew Chem Int
1103 Ed Engl, 54: 10313-6.

1104 Wu, J. X., Y. S. Cheng, J. Wang, L. Chen, M. Ding, and J. W. Wu. 2015. 'Structural
1105 insight into the mechanism of synergistic autoinhibition of SAD kinases', Nat Commun,
1106 6: 8953.

1107 Xiao, H., M. P. Jedrychowski, D. K. Schweppe, E. L. Huttlin, Q. Yu, D. E. Heppner, J. Li,
1108 J. Long, E. L. Mills, J. Szpyt, Z. He, G. Du, R. Garrity, A. Reddy, L. P. Vaites, J. A.
1109 Paulo, T. Zhang, N. S. Gray, S. P. Gygi, and E. T. Chouchani. 2020. 'A Quantitative
1110 Tissue-Specific Landscape of Protein Redox Regulation during Aging', Cell, 180: 968-83
1111 e24.

1112 Yeung, W., A. Kwon, R. Taujale, C. Bunn, A. Venkat, and N. Kannan. 2021. 'Evolution
1113 of Functional Diversity in the Holozoan Tyrosine Kinome', Molecular Biology and
1114 Evolution, 38: 5625-39.

1115 Yoshida, H., and M. Goedert. 2012. 'Phosphorylation of microtubule-associated protein
1116 tau by AMPK-related kinases', J Neurochem, 120: 165-76.

1117 Zmijewski, J. W., S. Banerjee, H. Bae, A. Friggeri, E. R. Lazarowski, and E. Abraham.
1118 2010. 'Exposure to hydrogen peroxide induces oxidation and activation of AMP-
1119 activated protein kinase', J Biol Chem, 285: 33154-64.

1120
1121
1122
1123
1124
1125
1126
1127
1128
1129
1130
1131
1132
1133
1134
1135

1136

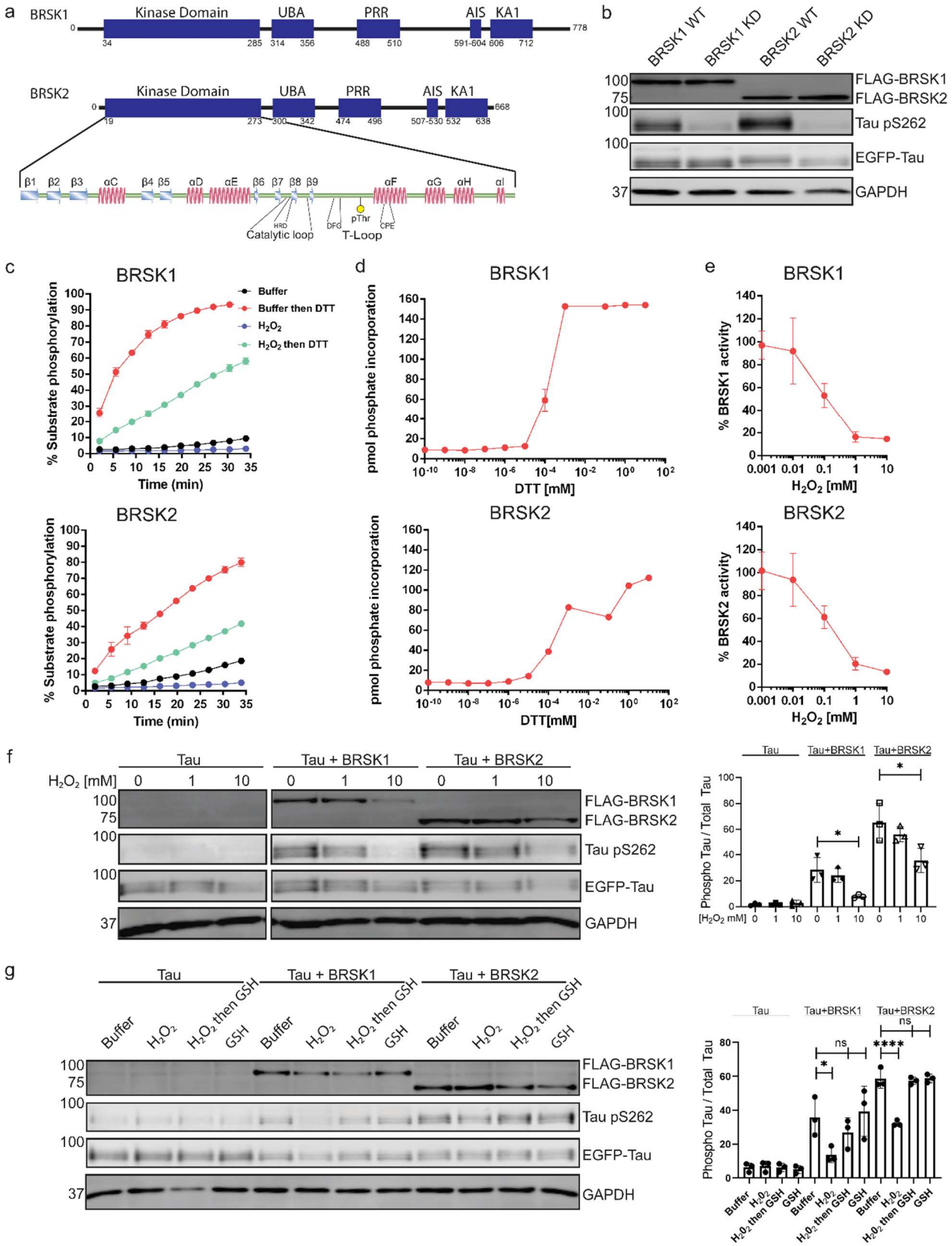
a
BRSK1
Kinase Domain
UBA
PRR
AIS
KA1
BRSK2
Catalytic loop
T-Loop
b
BRSK1 WT
BRSK1 KD
BRSK2 WT
BRSK2 KD
FLAG-BRSK1
FLAG-BRSK2
Tau pS262
EGFP-Tau
GAPDH
c
BRSK1
Buffer
Buffer then DTT
H2O2
H2O2 then DTT
% Substrate phosphorylation
Time (min)
BRSK2
d
pmol phosphate incorporation
DTT [mM]
e
% BRSK1 activity
% BRSK2 activity
H2O2 [mM]
f
Tau
Tau + BRSK1
Tau + BRSK2
H2O2 [mM]
Phospho Tau / Total Tau
g
Buffer
H2O2
H2O2 then GSH
GSH
ns
****

1137 Figure 1: BRSK1/2 are redox sensitive. (a) Schematic representation of BRSK domain
1138 architecture, including Kinase domain, Ubiquitin Associated (UBA) domain,
1139 Proline-Rich Region (PRR), Kinase Associated Domain(KA1), and Autoinhibitory
1140 Sequence (AIS). (b) Immunoblotting showing BRSK dependent phosphorylation
1141 of Tau at Ser262 (pS262), from lysates of HEK-293T cells overexpressing full-
1142 length FLAG-BRSK1 or 2 (wild type [WT] or kinase dead [KD]) and EGFP-Tau.
1143 (c) Real time phosphorylation of fluorescent AMARA peptide by full length
1144 BRSK1 and 2 (200 ng) purified from Sf21 cells. BRSK proteins were incubated
1145 with buffer or 1 mM H_2O_2 for 10 mins, reactions were then initiated with the
1146 addition of ATP and peptide substrate in the presence (where indicated) of 10
1147 mM DTT. Dose response curves for (d) DTT and (e) H_2O_2 with 200 ng full-length
1148 BRSK1 and BRSK2. All kinases assays are shown as mean and SD of three
1149 experiments. (f) Immunoblott (left) of pS262 in transiently co-transfected HEK-
1150 293T cells incubated with the indicated concentration of H_2O_2 for 10 mins. Signal
1151 density for phospho Tau S262 and total Tau (GFP) was obtained using
1152 ImageStudio software (Licor) and results from at least 3 biological replicates
1153 were anaylzed with Graphpad Prism software using one way anova to determine
1154 significance. Data shown is mean and SE. (g) Representative immunoblot (left)
1155 of transiently co-transfected HEK-293T cells treated with 10 mM H_2O_2 for 10
1156 mins before the addition of 20 mM GSH. Whole cell lysates were harvested after
1157 a further 15 mins. Normalized densitometry of Tau pS262 signal (right) was
1158 calculated from 3 independent experiments. Data shown is mean and SD. * = $P < 0.05$, **= $P < 0.01$, ***= $P < 0.001$.

1160

a

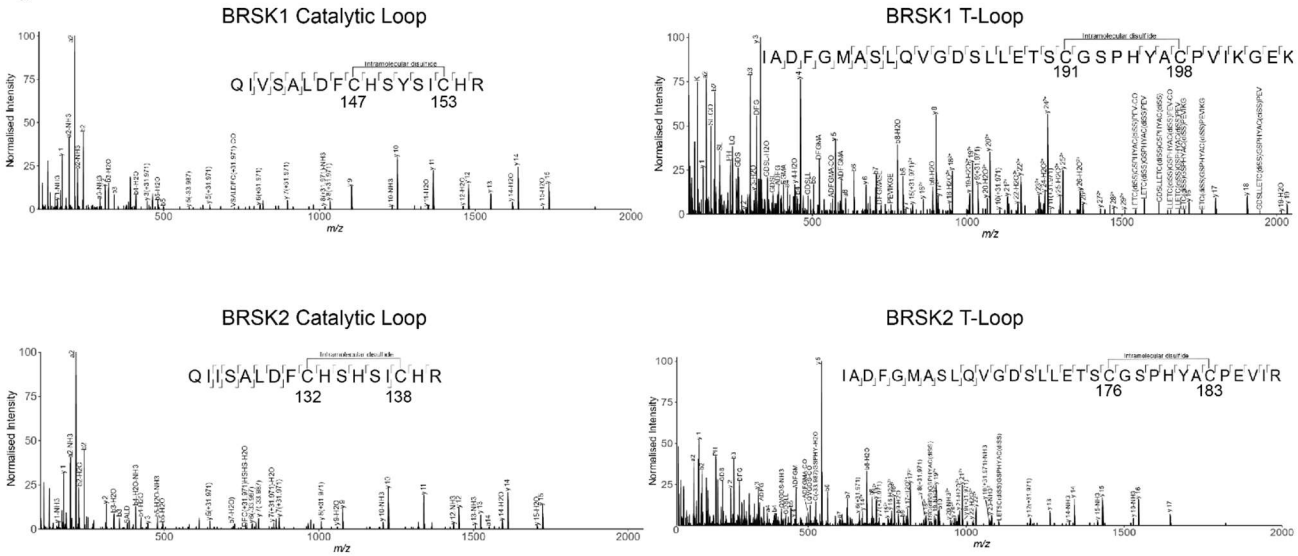
BRSK1 Catalytic Loop
Q I V S A L D F C H S Y S I C H R
147
153
BRSK1 T-Loop
I A D F G M A S L Q V G D S L L E T S C G S P H Y A C P V I K G E K
191
198
BRSK2 Catalytic Loop
Q I I S A L D F C H S H S I C H R
132
138
BRSK2 T-Loop
I A D F G M A S L Q V G D S L L E T S C G S P H Y A C P E V I R
176
183
Normalised Intensity
m/z

b

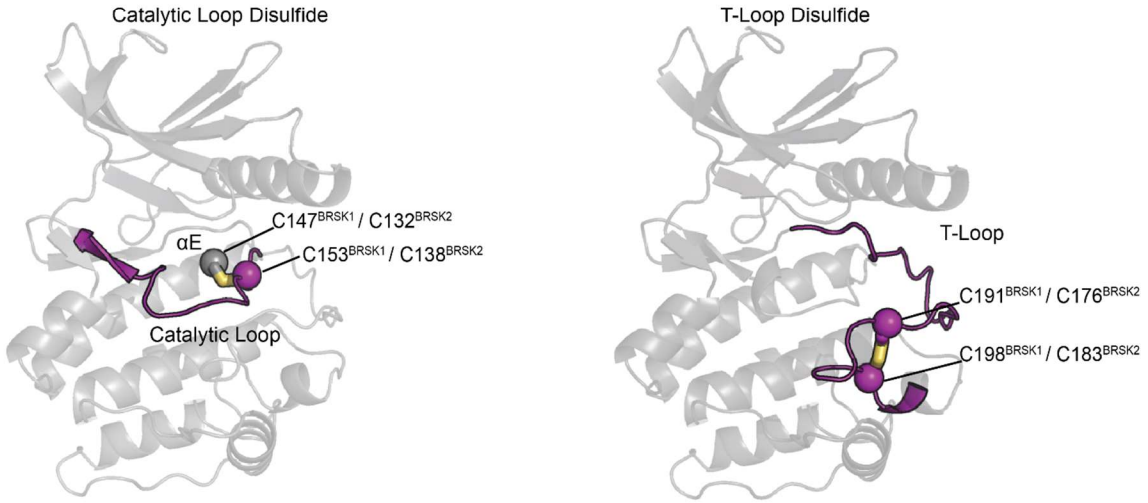
Catalytic Loop Disulfide
αE
C147BRSK1 / C132BRSK2
C153BRSK1 / C138BRSK2
Catalytic Loop
T-Loop Disulfide
T-Loop
C191BRSK1 / C176BRSK2
C198BRSK1 / C183BRSK2

c

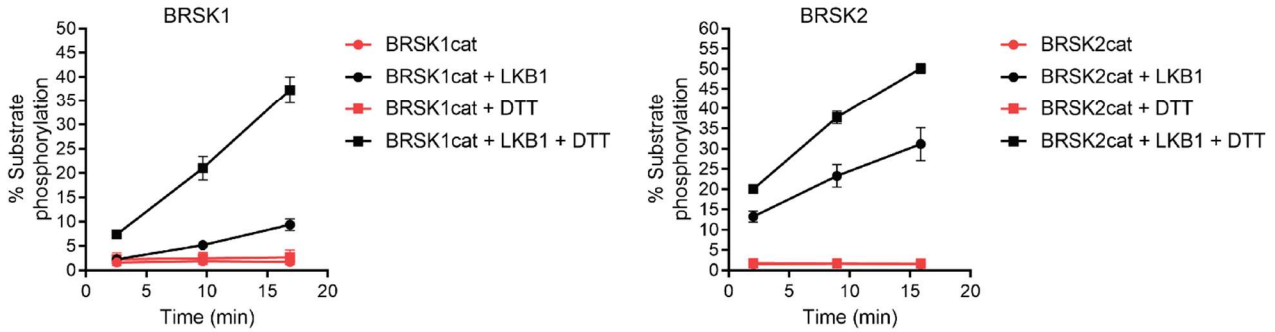
BRSK1
% Substrate phosphorylation
Time (min)
BRSK1cat
BRSK1cat + LKB1
BRSK1cat + DTT
BRSK1cat + LKB1 + DTT
BRSK2
BRSK2cat
BRSK2cat + LKB1
BRSK2cat + DTT
BRSK2cat + LKB1 + DTT

1161 Figure 2: Intramolecular disulfide bonds form in the kinase domains of BRSK1 and 2. (a)
1162 Full length BRSK1 and 2 were affinity-purified from HEK-293T cells and
1163 subjected to LC-MS/MS analysis. LC-MS/MS spectrum mapping revealed
1164 disulfide bridges formation between $C147^{BRSK1}$ - $C153^{BRSK1}$, $C191^{BRSK1}$ -
1165 $C198^{BRSK1}$, $C132^{BRSK2}$ - $C138^{BRSK2}$, and $C176^{BRSK2}$ - $C183^{BRSK2}$. Peptide
1166 coverage was 74 and 78 % for BRSK1 and BRSK2 respectively. (b) Alphafold
1167 structures demonstrating the location of disulfide bonds within the kinase
1168 domains of BRSK1 and BRSK2. (c) Real time phosphorylation of fluorescent
1169 AMARA peptide by the kinase domains of BRSK1 and 2 (100 ng) purified from
1170 *E.coli* . BRSK1 (29-358) and BRSK2 (14-341) were activated by incubation with
1171 LKB1 and assayed in the presence or absence of 1 mM DTT.

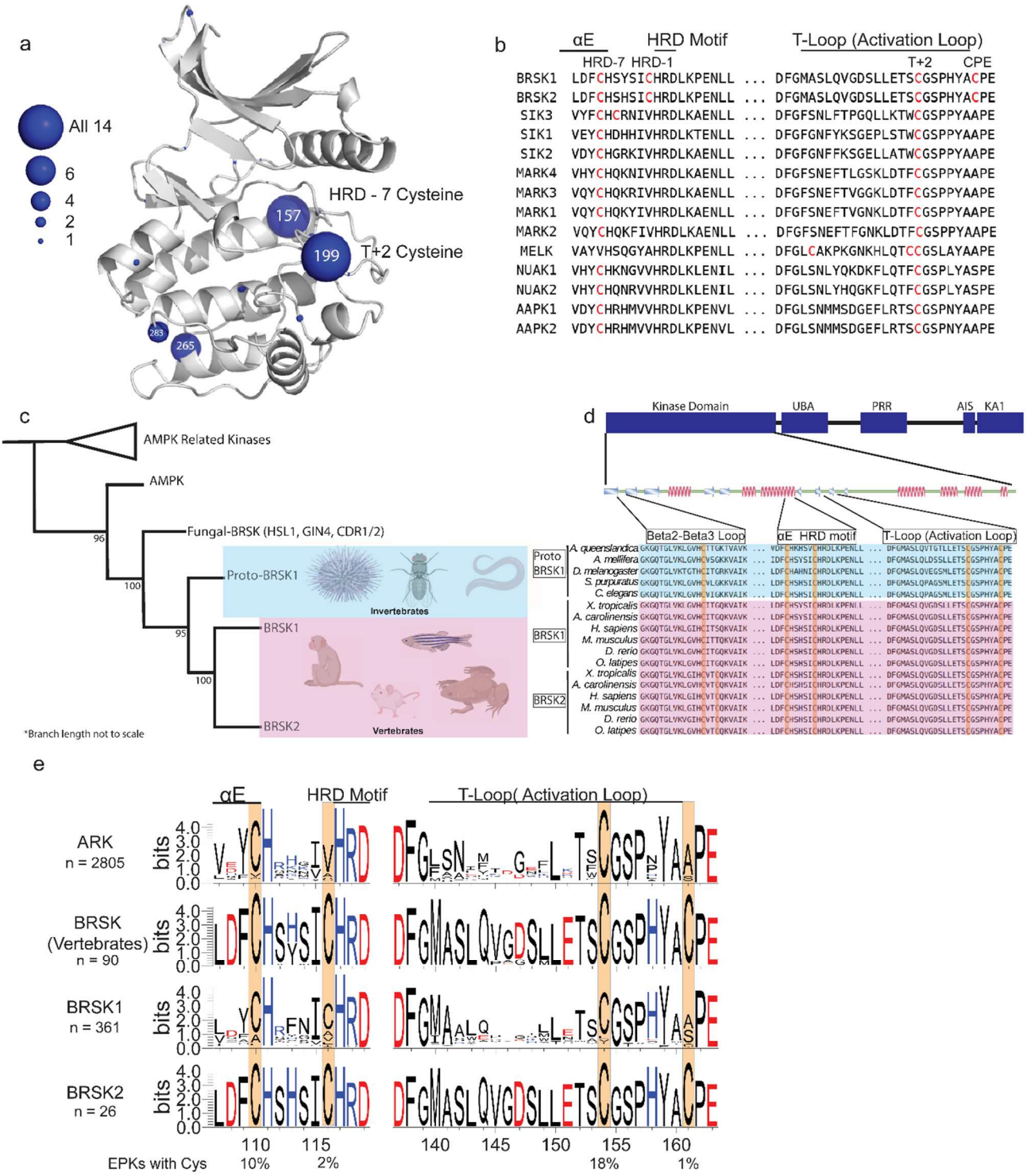

Figure 3: Cysteine pairs are highly conserved within the activation segments of BRSKs. (a) Mapping of Cys residues (spheres) in the kinase domains of human ARK family members. Numbers represent the corresponding amino acid position in

PKA. Sphere size is proportional to the number of ARKs that contain a Cys at a specific site. (b) Activation segment sequence alignment of the 14 human ARKs. (c) Phylogenetic analysis showing divergence and grouping of BRSKs sub-families in different taxonomic groups. Bootstrap values are included for each clade. (d) Sequence alignment of the kinase domains of invertebrate and vertebrate BRSKs. (e) Analysis of relative amino acid conservation in ARKs and BRSKs, centered on the HRD containing catalytic loop, and the T-loop (between the DFG and APE motifs). Data is presented as HMM (hidden Markov models) Sequence Logos. The % of ePKs that possess a specific Cys is shown at the bottom.

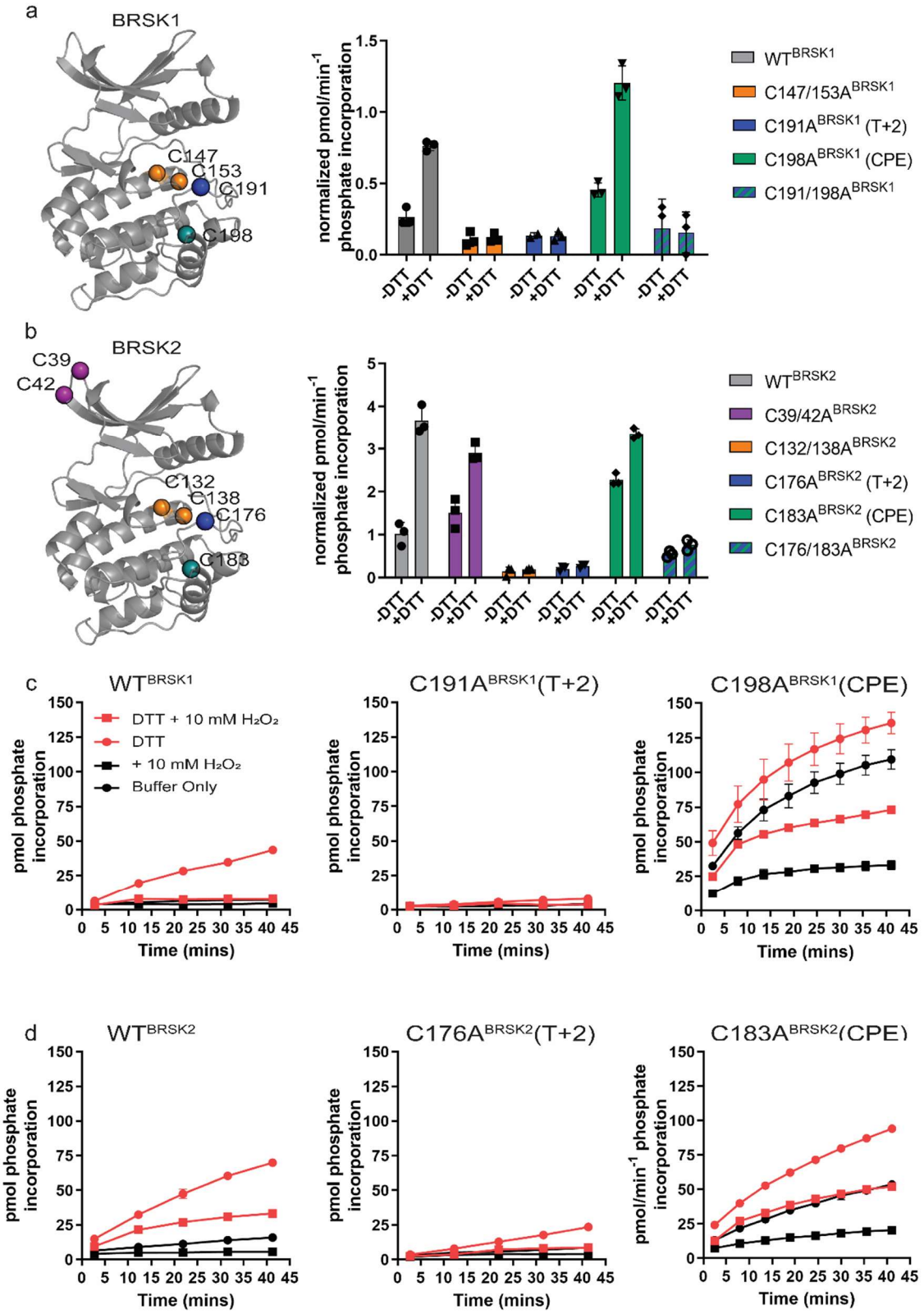
a
BRSK1
C147
C153
C191
C198
normalized pmol/min-1 phosphate incorporation
WTBRSK1
C147/153ABRSK1
C191ABRSK1 (T+2)
C198ABRSK1 (CPE)
C191/198ABRSK1
-DTT
+DTT
b
BRSK2
C39
C42
C132
C138
C176
C183
WTBRSK2
C39/42ABRSK2
C132/138ABRSK2
C176ABRSK2 (T+2)
C183ABRSK2 (CPE)
C176/183ABRSK2
c
WTBRSK1
C191ABRSK1(T+2)
C198ABRSK1(CPE)
DTT + 10 mM H2O2
DTT
+ 10 mM H2O2
Buffer Only
pmol phosphate incorporation
Time (mins)
d
WTBRSK2
C176ABRSK2(T+2)
C183ABRSK2(CPE)
pmol/min-1 phosphate incorporation

1186

1187

1188 Figure 4: Cysteine residues within the kinase domain fine-tune BRSK activity. In vitro
1189 kinase assays (right panels) showing normalized rates of peptide
1190 phosphorylation by WT and Cys-to-Ala variants of (a) BRSK1 and (b) BRSK2.
1191 100 ng of LKB1 activated BRSK kinase domain was assayed in the presence or
1192 absence of 1 mM DTT. The positions of mutated Cys residues are modelled on
1193 the kinase domain as coloured spheres (left panel). Real time in vitro assays
1194 using (c) 50 ng BRSK1 and (d) 20 ng BRSK2. LKB1-activated BRSK proteins
1195 were incubated on ice in the presence or absence of 250 μM DTT for 30 mins.
1196 Assays were initiated by the addition of ATP and fluorescent peptide substrate in
1197 the presence or absence of 1 mM H_2O_2. All data is mean and SD of 3
1198 experiments and activities are normalized to LKB1-phosphorylated BRSK signal
1199 (Supp Fig 4 b).
1200

1201

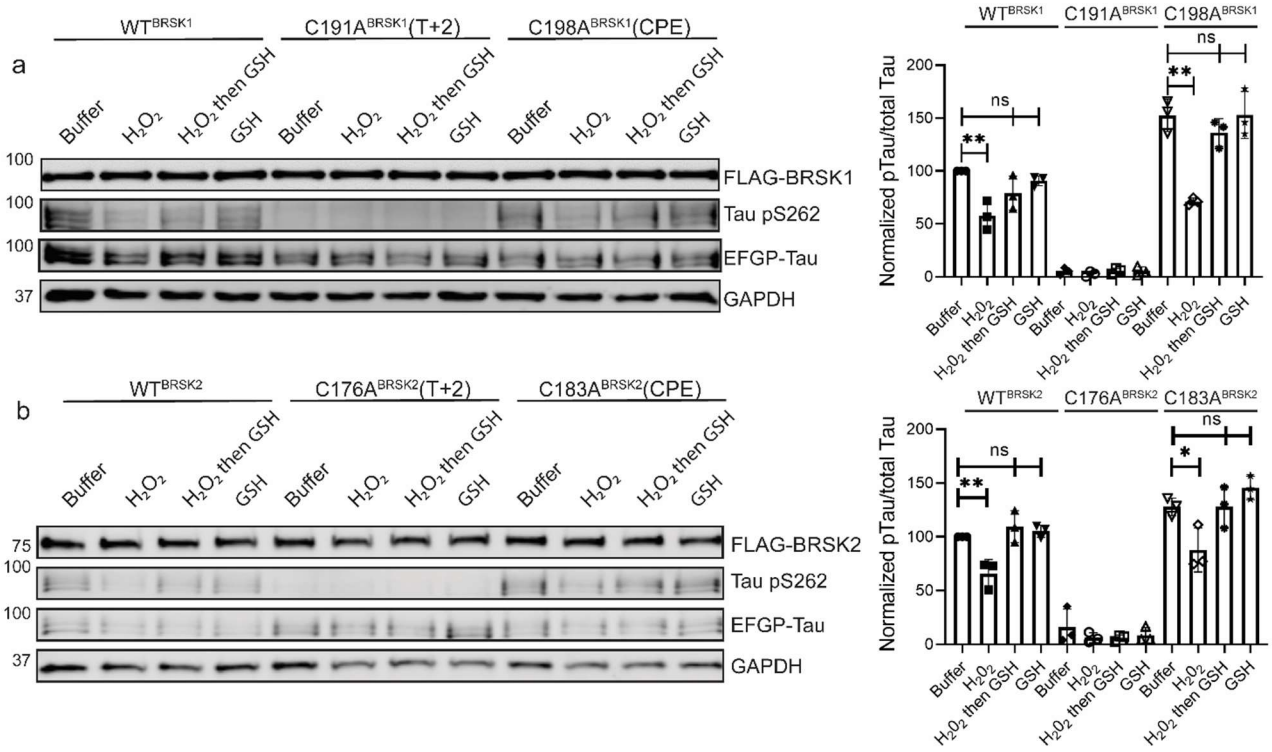

1202

1203 Figure 5: Impact of T-Loop and CPE Cys-to-Ala mutations on BRSK redox sensitivity in
1204 a cellular EGFP-Tau HEK-293T co-expression system. Representative
1205 immunoblot of EGFP-Tau co-expressed with WT and Cys-to-Ala mutants of (a)
1206 BRSK1 and (b) BRSK2 (left panels). Transiently transfected HEK-293T cells
1207 were treated with or without 10 mM H_2O_2 for 10 mins before the addition of 20

mM GSH. Whole cell lysates were harvested after a further 15 mins. Signal density for phospho Tau S262 and total Tau (GFP) was obtained using ImageStudio software (Licor) and results from at least 3 biological replicates were anaylzed with Graphpad Prism software using one way anova to determine significance (right panels). Data shown is mean and SE. All values are normalized to Tau pS262 signals from control (buffer only treatment) WT BRSK and Tau co-transfections. Data shown is mean and SD. * = P < 0.05, **= P < 0.01, ***= P < 0.001.

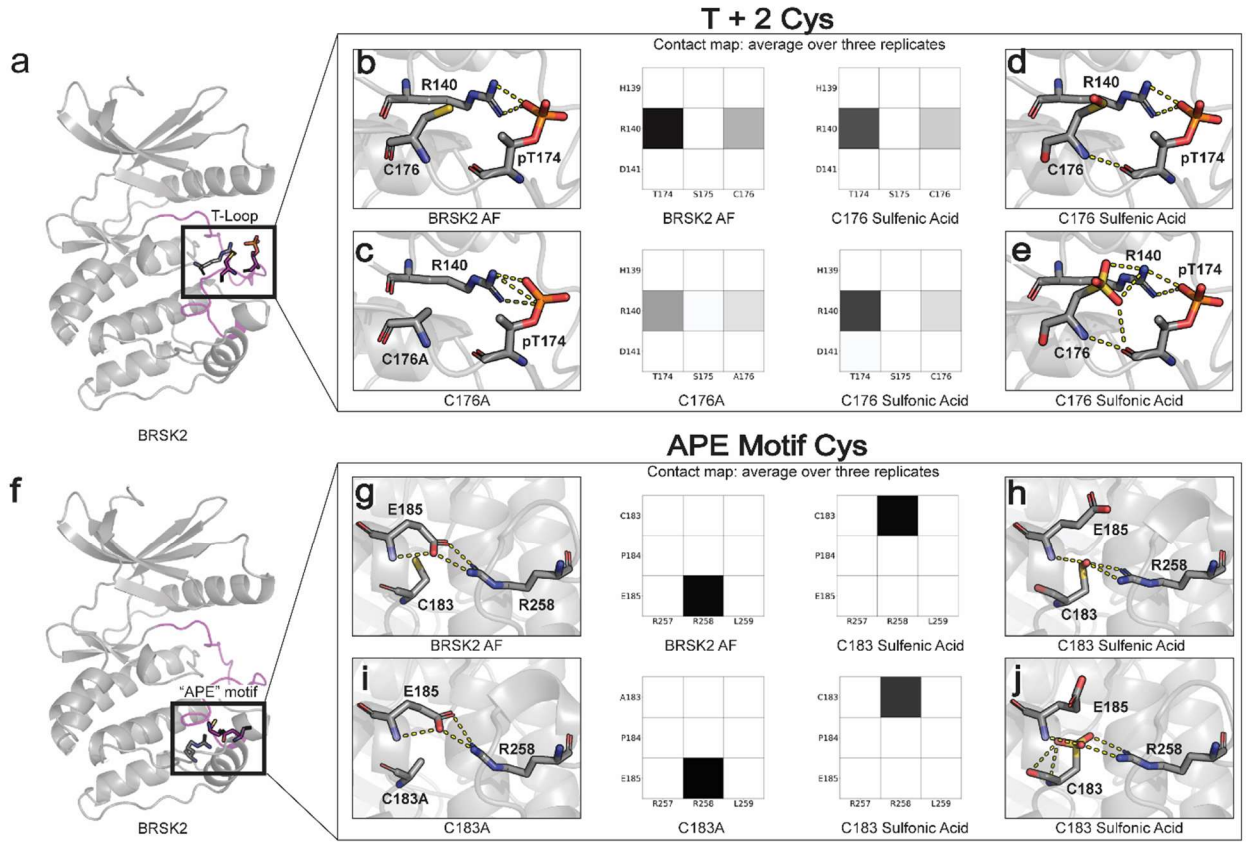

Figure 6: Oxidative cysteine modifications alter critical structural interactions required for BRSK allosteric regulation. Three replicates of 100 ns GROMACS molecular dynamics simulations were performed to evaluate the effects of cysteine mutation and oxidation. Salt bridge disruption was analyzed by generating contact maps representing the percentage of the simulation time in which residues were within appropriate distance (3 Angstroms). (a) T+2 Cys is located in proximity to the activation loop threonine in the T loop. (b-e) Evaluation of pT174-R140 salt bridge formation in wild type, C176A, and oxidized C176 BRSK2. (f) Location of CPE salt bridge within BRSK2. (g-j) Evaluation of E185-R258 salt bridge formation in wild type, C183A, and oxidized C183 BRSK2.

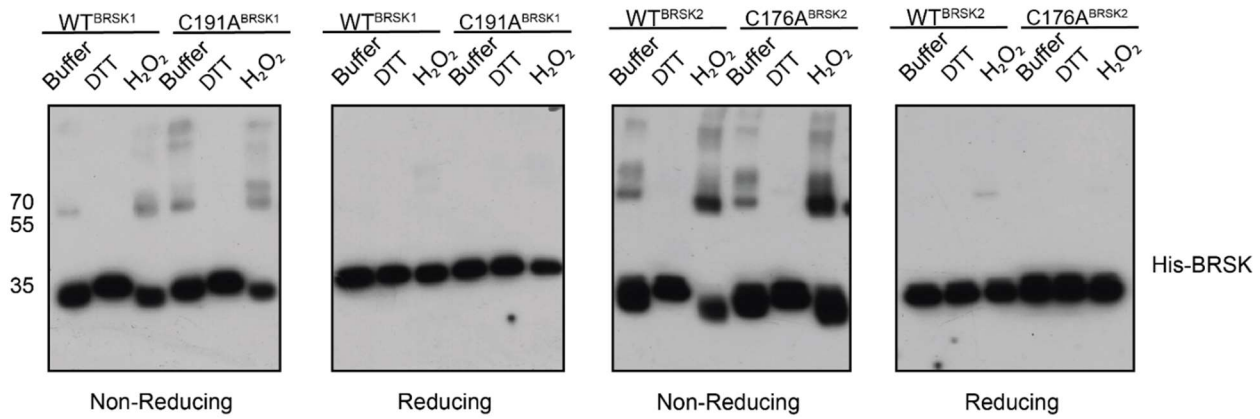

Figure 7: BRSK1/2 form limited disulfide-mediated multimers. Western blot analysis of BRSK1/2 kinase domain purified from *E. coli* and incubated with buffer, H_2O_2, or DTT and subjected to non-reducing or reducing PAGE to evalute the formation of intramolecular disulfide bonds.

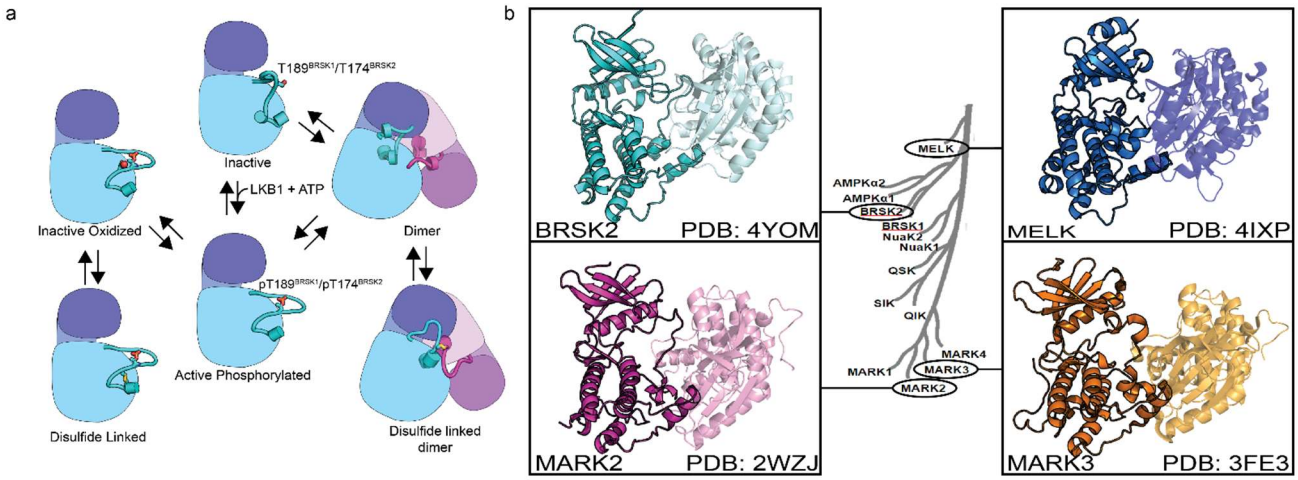

Figure 8: (a) Model of BRSK1/2 regulation. Schematic diagram demonstrating ways in which residues within BRSK kinases permit fine-tuning of catalytic activity through a variety of oxidative modifications, potentially including inter and intramolecular disulfide bonds. Cartoon representation of kinase domain with N-lobe colored dark blue/purple and the C-lobe colored light blue/purple. (b) ARK family member crystal structures demonstrate the ability to form asymetric dimers bringing T + 2 cys into proximity. Crystal structures for MARK2 and MELK both contain intermolecular disulfide bonds between T + 2 cys.